AECD - 2570

UNITED STATES ATOMIC ENERGY COMMISSION

LOW-ENERGY CROSS SECTION OF THE D-D REACTION AND ANGULAR DISTRIBUTION OF THE PROTONS EMITTED

by

E. Bretscher
A. P. French

Los Alamos Scientific Laboratory

Date of Manuscript: September 17, 1946
Date Declassified: April 18, 1949

Technical Information Division, ORE, Oak Ridge, Tennessee
AEC, Oak Ridge, Tenn., 2-24-50--850-A9339

PRINTED IN USA
PRICE 20 CENTS

DISCLAIMER NOTICE

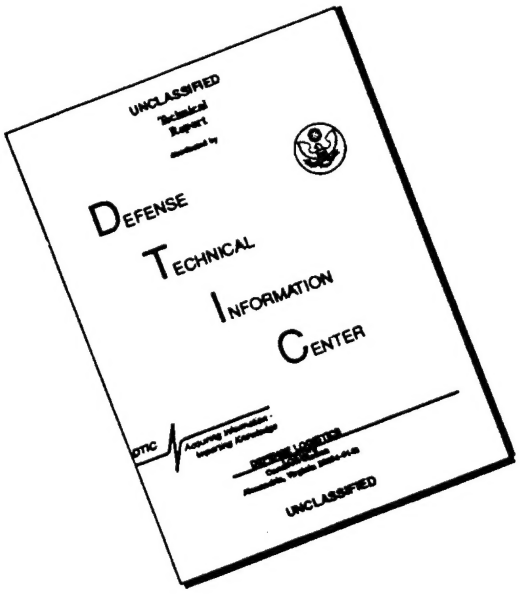

THIS DOCUMENT IS BEST QUALITY AVAILABLE. THE COPY FURNISHED TO DTIC CONTAINED A SIGNIFICANT NUMBER OF PAGES WHICH DO NOT REPRODUCE LEGIBLY.

LOW-ENERGY CROSS SECTION OF THE D-D REACTION AND ANGULAR DISTRIBUTION OF THE PROTONS EMITTED

By E. Bretscher and A. P. French

ABSTRACT

The thick-target yield of the reaction D + D → T + p + 3.98 Mev has been measured, using a heavy-ice target, and observations have been made on the angular distribution of the protons. Experiments have been carried out in the region 15 Kev to 105 Kev incident deuteron energy. Evidence has been obtained that, even for very small bombarding energies, the angular distribution of protons in the center-of-gravity (c.g.) system does not become isotropic. The variation of the cross section with energy can only approximately be represented by a Gamow function.

Introduction

The quantity which is determined in the experiments is the total number of disintegrations as a function of the bombarding energy. The cross section is then obtained from the slope of the excitation curve. If the thick-target yield at bombarding energy E is denoted by N(E), one has:

$$\sigma(E) = \frac{1}{A} \cdot \frac{dN}{dE} \cdot \frac{dE}{dx}$$

where the constant A contains the product of the number of incident deuterons per unit of beam current and the number of deuterium nuclei per cm^3 of the target. dE/dx is the rate of energy loss of the incident deuterons in the target. In another report (LAMS-392) the energy loss of protons and deuterons in D_2O is discussed. Numerical values are there quoted for dE/dx in D_2O vapour. By suitable adjustment of the constant A, these values can be inserted in the above formula to determine $\sigma(E)$. One finds:

$$\sigma(E) = 2.38 \times 10^{-6} \frac{dN}{dE} \cdot \frac{dE}{dx} \text{ barns,}$$

where N(E) = thick target yield per microcoulomb of incident deuterons,
dN/dE = change of N(E) per Kev change of bombarding energy,
dE/dx = rate of energy loss in Kev per cm of deuterons in D_2O vapour at 1 mm pressure, 15°C.
The experiments described in what follows are concerned with the determination of N(E).

Apparatus.

(a) High-voltage Equipment

The first experiments were made in the region 15 to 50 kev bombarding energy. For this purpose a small full-wave rectifier set was constructed. The circuit is shown in Fig. 1. The general layout of the accelerating system, together with focusing electrode and ion source, is shown diagrammatically in Fig. 2.

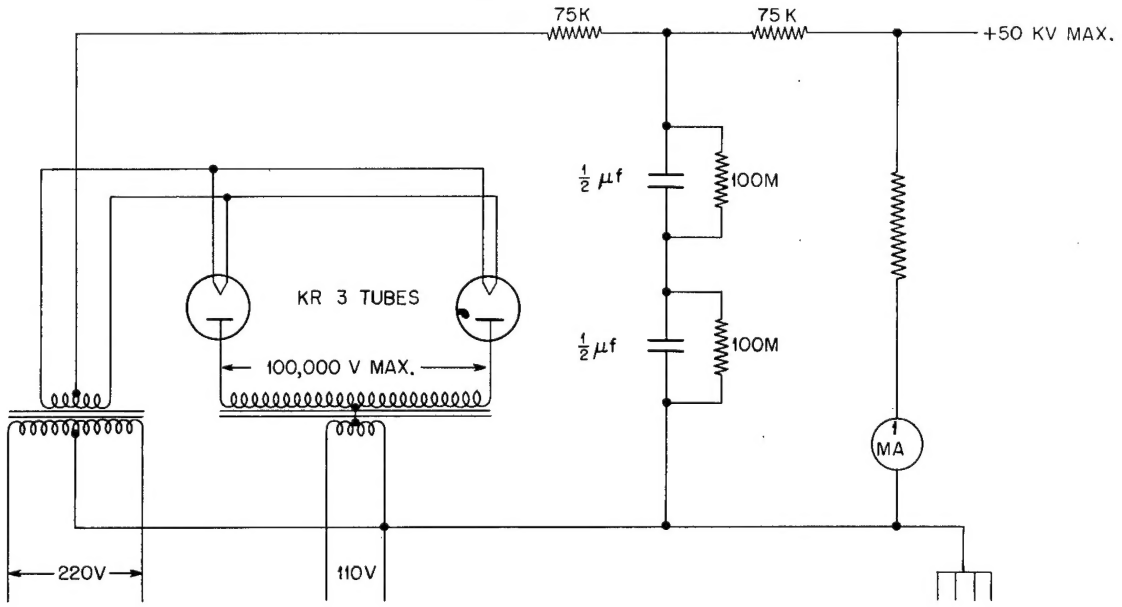

Figure 1. Circuit diagram of 50 kv set (full wave rectifier).

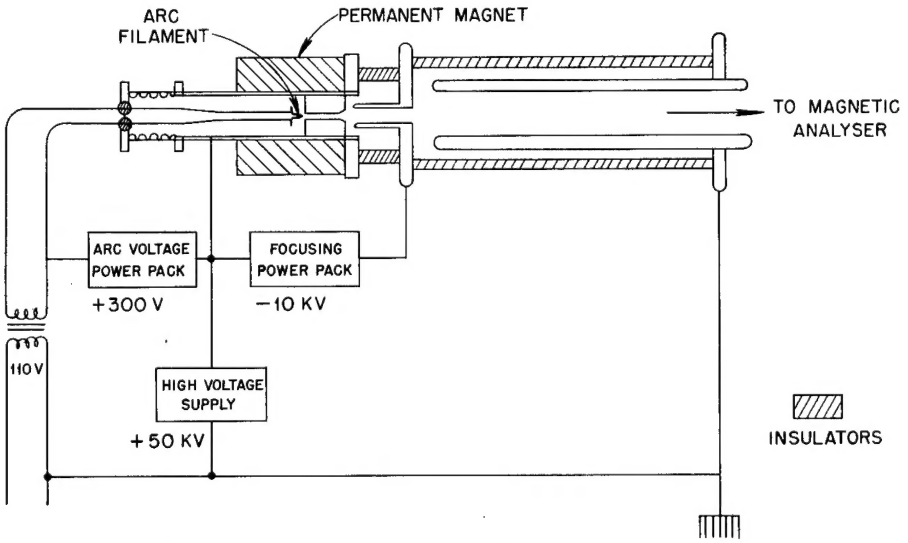

Figure 2. Ion source and accelerating system. (50 kv set).

It was later found desirable to extend the measurements to higher energies, and a second high-voltage set was built, for voltages up to 125 kev. This was a voltage doubler; the circuit is shown in Fig. 3. The arrangement of ion source, focusing electrodes and accelerating system is represented in Fig. 4.

On both accelerating systems a 4" oil diffusion pump was mounted at the ground potential end, i.e., in the region traversed by the deuterons after full acceleration and before magnetic analysis. In this way practically none of the gas admitted to the ion source reached the magnetic analyser.

(b) Ion Sources

In conjunction with the smaller set the ion source shown in Fig. 5 was used. The construction is simple and will not be described here. A cylindrical permanent magnet was used to lengthen the electron path for ionizing collisions in the canal.

For the larger set an essentially similar source was made. (Fig. 6). In this, however, an electromagnet was used for controlling the electron paths, and this provided an additional adjustment for obtaining optimum beam currents.

Both sources were based on a design of a familiar type, and differed only in minor constructional details from models already in use.

(c) Target Chamber and Counter

The vacuum chamber—the "tank"—is shown in Figs. 7 and 8. It is a cylindrical brass box with a steel lid, and is maintained at a low pressure (a few units of 10^{-6} mm) by a 4" oil diffusion pump mounted below it. Most of the salient features are indicated in the plan (Fig. 7). After acceleration through the bombarding potential, the deuteron beam was magnetically analyzed between the poles of an electromagnet was a vertical field, in order to select D_1^+ or D_2^+ ions of a specified velocity. The beam was then collimated and entered the tank along a horizontal radius. It passed between a pair of electro-static analyzer plates (used to test for the presence of neutral particles in the beam, but normally kept grounded) and impinged upon the target.

The target consisted of a copper plate whose plane was vertical. It was soldered to the under side of a liquid nitrogen container, which in turn was supported on a thin-walled steel tube passing through a Wilson seal in the lid of the tank. The target could thus be rotated. The axis of rotation coincided with the vertical axis of the tank itself, and was carefully arranged to lie in the front face of the target plate. Under these circumstances, the spot produced at the front face of the target by a radial beam lay always on the axis of the tank, and did not change its position as the target was rotated.

After the cooling trap had been filled, a layer of heavy ice could be deposited on the target, which could then be turned to any desired orientation for carrying out a measurement.

The protons from the nuclear reaction were detected in proportional counter (Fig. 9), having a mica window of about 8 cms air equivalent. (The proton range was about 14 cms; all other charged particle ranges were less than 2 cms). The counter window subtended a small fraction, about 1/1000, of 4π at the target spot. The arrangement was therefore one having 'good' geometry. The counter could be rotated in a horizontal plane about a vertical axis passing through the target spot. The adjustment was made through a Wilson seal at the bottom of the tank (Fig. 8), so that the position of the counter could be altered without breaking the vacuum. The 'setting' of the counter, defined as the angle between the direction of the incident beam and the radius joining target spot to counter window, could be varied from 40° to 150° for the study of the angular distribution of the protons. The counter was enclosed in a grounded copper shield; before this was done it tended to pick up stray disturbances from the target, which, when connected to the input of the beam current integrator, had a very high impedance to ground.

Two glass windows were provided in the tank to permit an optical check on the alignment of the system.

A large auxiliary cooling trap (Fig. 7) was placed in the tank above the wide tube leading to the diffusion pump. It was kept filled with liquid nitrogen for several hours before a run, serving to clean up the vacuum and to prevent the escape of any oil vapour from the pump into the tank.

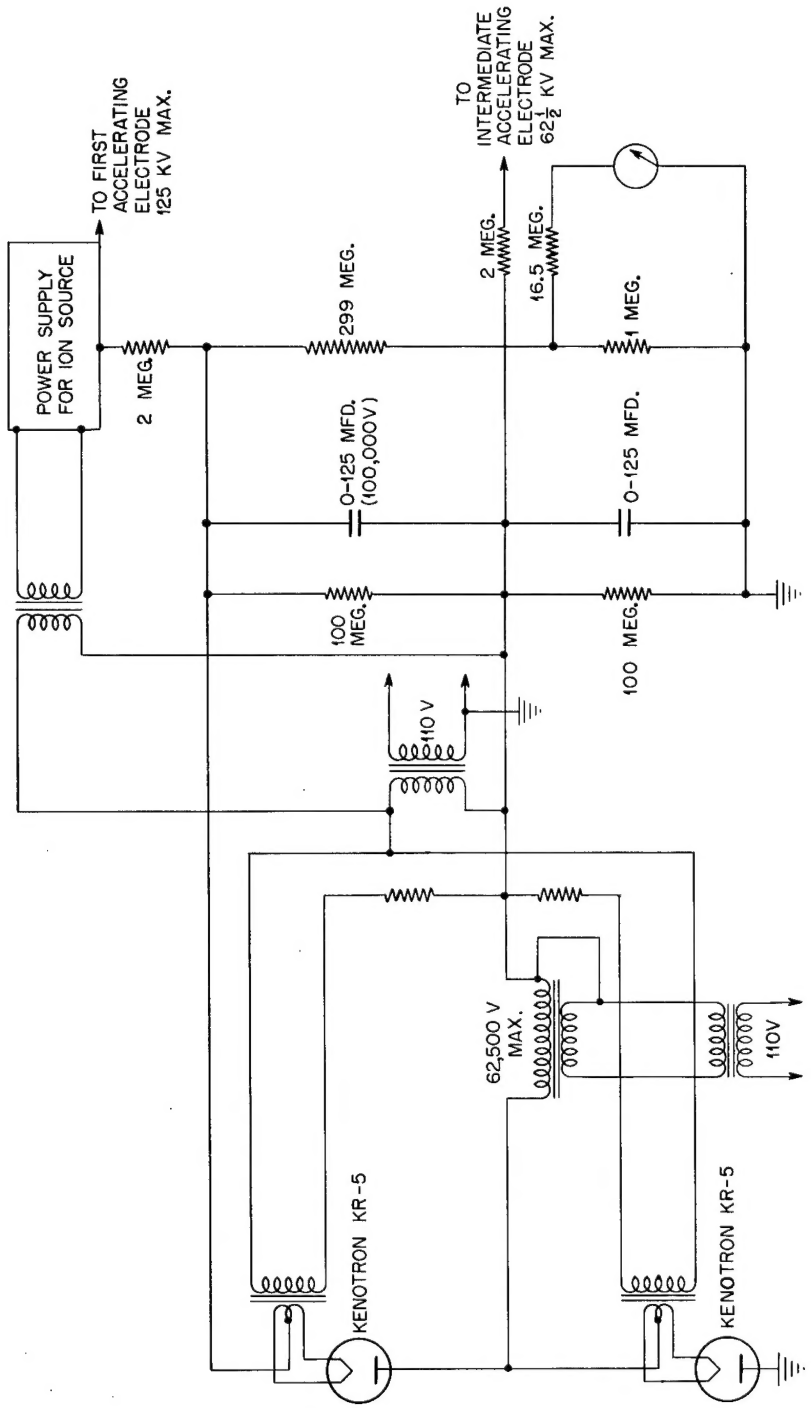

Figure 3. Circuit diagram of 125 kv set (voltage doubler).

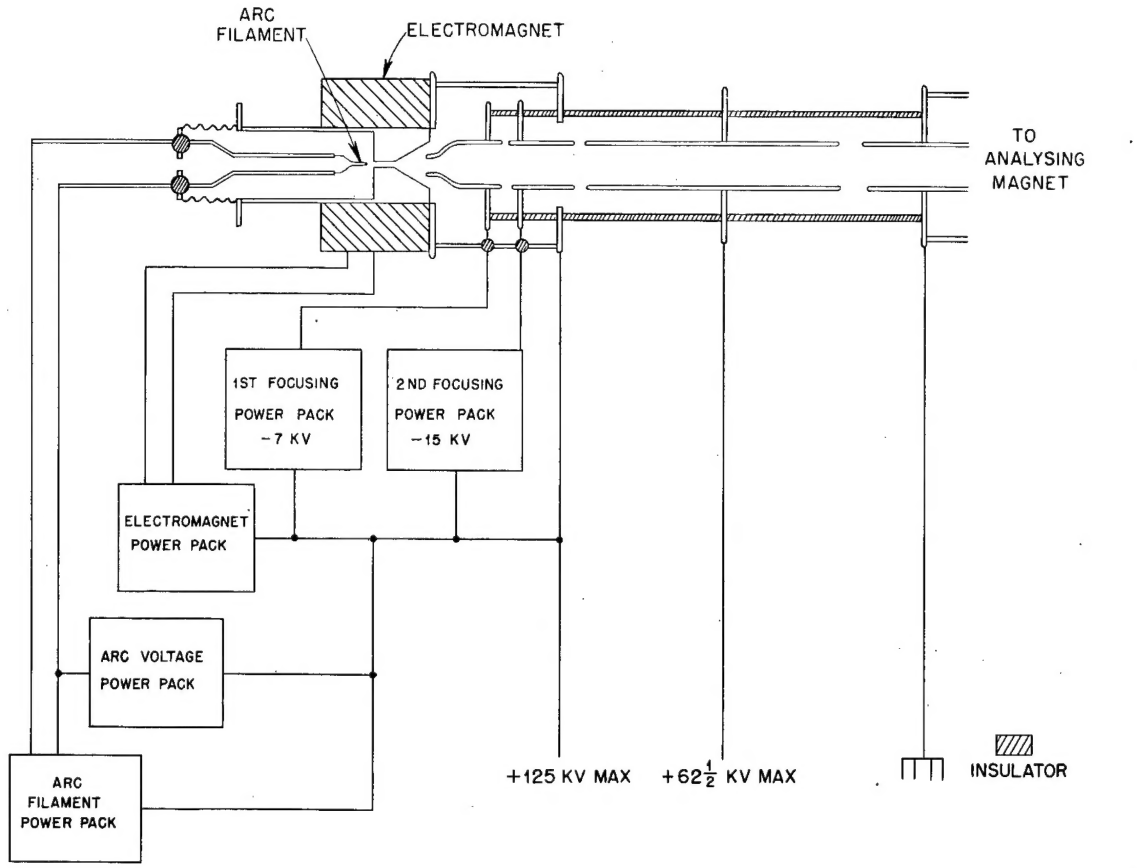

Figure 4. Ion source and accelerating system (125 kv set).

(d) Current Integrator

The accurate measurement of beam currents was fundamental to the evaluation of N(E). The use of a valvanometer for the purpose was undesirable since the current to be measured was sometimes small, and a galvanometer sensitive enough to measure it could not follow sudden variations in its magnitude.

A current integrator, for use in the range 0.01 to 2.5 microamp, was therefore designed by M. P. Poole. The circuit diagram is shown in Fig. 10. Apart from an extensive use of electronic instead of mechanical relays, it was similar to existing designs. A careful selection of tubes for the circuit, together with a balancing of leakage current effects, made the integrator useful down to quite low currents. Its calibration (Fig. 11), effected with the aid of a galvanometer, suggested no change of sensitivity due to leakage current, even for an input current of only 5.10^{-3} microamp.

Charge was accumulated on a .005 microfarad silver mica condenser, which was automatically discharged when the potential reached about 100 volts. Thus to measure, correct to 1%, an input current of 0.1 microamp, the input impedance needed to be 10^5 megohms (to make the mean leakage current less than 10^{-3} microamp). Care was taken to ensure that the target insulation to ground was better than this.

The calibration of the integrator remained constant to ± 2%.

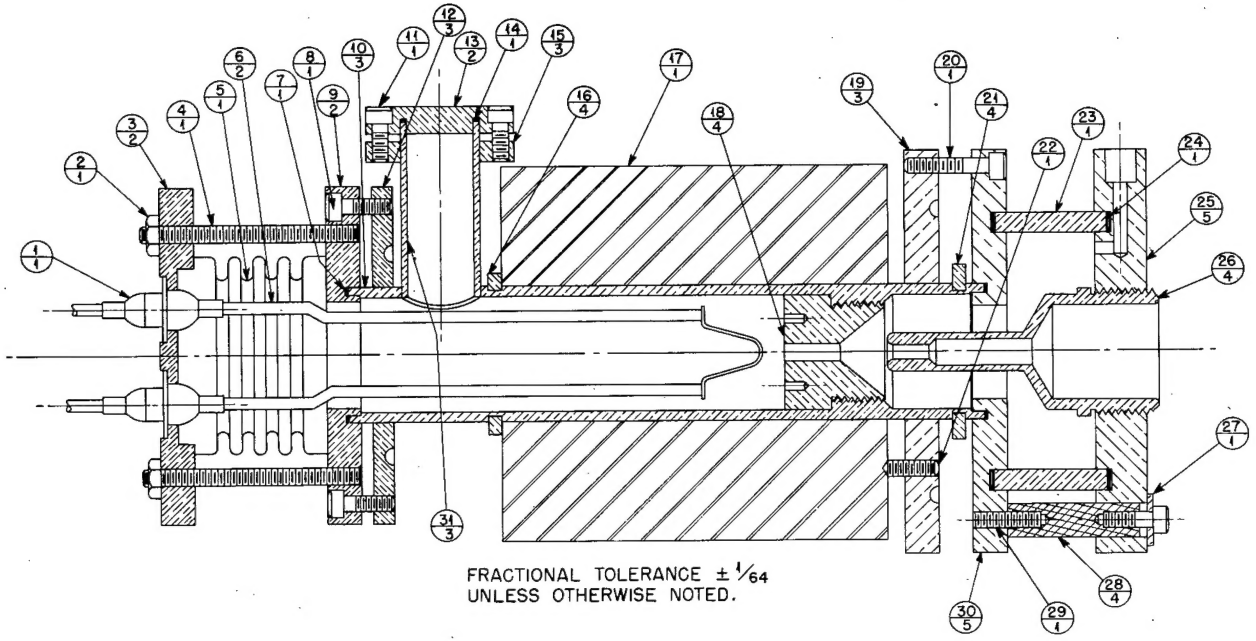

LIST OF PARTS

NO.	NAME AND DESCRIPTION	QUAN.	MATERIAL
1	KOVAR SEAL	3	COMM.
2	NO. 6 HEX NUT	4	BRASS
3	2 3/4 DIA. X 3/8 THK.	1	BRASS
4	NO. 6 STUD 1 5/8 LG.	4	BRASS
5	SYLPHON	1	COMM.
6	STEEL WIRE TO SUIT	1	COMM.
7	1 DIA. X 1/16 THK.	2	RUBBER
8	NO. 6 ALLEN HD. CAP SC.	6	BRASS
9	2 3/4 DIA. X 3/8 THK.	1	BRASS
10	1 1/8 O.D. X 5/8 I.D. TUB.	1	BRASS
11	NO. 6 ALLEN HD. CAP SC.	6	BRASS
12	2 3/4 DIA. X 1/4 THK.	1	BRASS
13	1 1/4 DIA. X 1/4 THK.	1	BRASS
14	.6 DIA. X 1/16 THK.	1	RUBBER
15	1 1/4 DIA. X 3/16 THK.	1	BRASS
16	1 1/4 O.D. X 1/8 THK.	1	BRASS
17	MAGNET	1	COMM.
18	1 DIA. X 7/8 LONG	1	BRASS
19	3 1/4 DIA. X 3/16 THK	1	BRASS
20	NO. 6 ALLEN HD. CAP SC.	6	BRASS
21	1 1/4 DIA. X 1/8 THK.	1	BRASS
22	NO. 6 ALLEN HD. SET SC.	3	BRASS
23	2 DIA. X 1/8 WALL	1	PORCELAIN
24	2 1/8 DIA. X 1/16 THK.	2	RUBBER
25	3 1/4 DIA. X 1/2 THK.	1	BRASS
26	1 DIA. X 2 1/8 LONG	1	BRASS
27	NO. 6 FLAT WASHER	6	BRASS
28	1/4 DIA. X 1 LONG	6	LUCITE
29	3 1/4 DIA. X 3/8 THK.	1	BRASS
30	3 1/4 DIA. X 3/16 THK.	1	BRASS
31	3/4 O.D. X 1/8 WALL TUBNG.	1	BRASS

DIMENSIONS ARE IN INCHES

Figure 5. Ion source (low voltage).

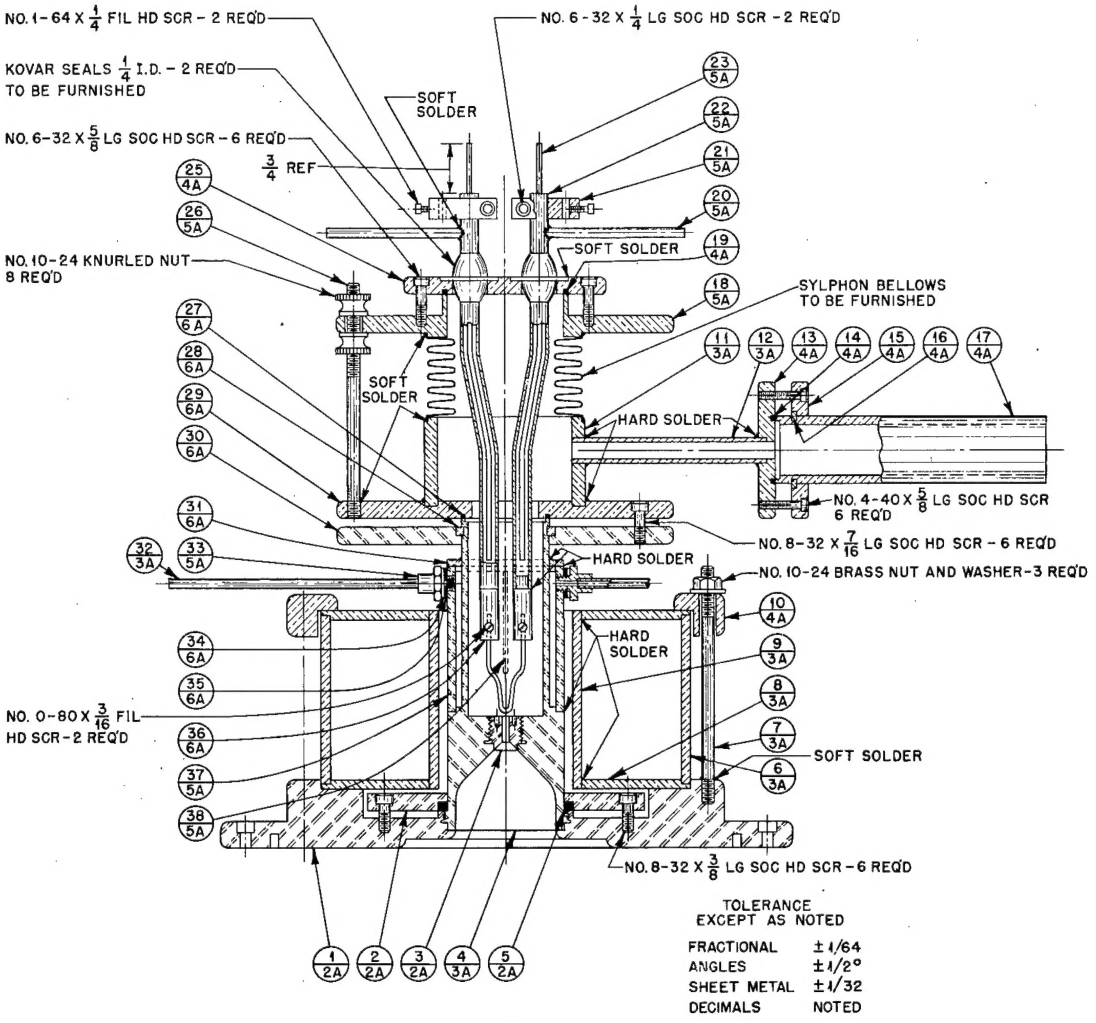

LIST OF PARTS

NO.	NAME AND DESCRIPTION	QUAN.	MATERIAL	NO.	NAME AND DESCRIPTION	QUAN.	MATERIAL
1	BASE	1	ST STL	20	TUBE	2	COPPER
2	COLLAR	1	ST STL	21	CLAMP BLOCK	2	BRASS
3	PLUG	3	ST STL	22	TUBE	2	COPPER
4	BODY	1	ST STL	23	TUBE	2	COPPER
5	GASKET	1	NEOPRENE	24	OMITTED	—	—
6	SHIELD	2	BRASS	25	CLAMP RING	1	BRASS
7	STUD	3	BRASS	26	STUD	4	BRASS
8	DISC	2	BRASS	27	GASKET	1	NEOPRENE
9	BUSHING	1	BRASS	28	CLAMP	1	ST STL
10	CLAMP RING	1	BRASS	29	COLLAR	1	BRASS
11	ADAPTER	1	BRASS	30	CLAMP RING	1	ST STL
12	TUBE	1	BRASS	31	COVER	1	ST STL
13	RING	1	BRASS	32	TUBE	2	COPPER
14	GASKET	1	NEOPRENE	33	FITTING	2	BRASS
15	CLAMP RING	1	BRASS	34	WASHER	2	BRASS
16	CLAMP	1	BRASS	35	SEAL	2	NEOPRENE
17	TUBE	1	BRASS	36	TERMINAL	2	BRASS
18	ADAPTER	1	BRASS	37	SLEEVE	1	ST STL
19	GASKET	1	NEOPRENE	38	BAFFLE	2	ST STL

Figure 6. Magnetic ion source, Model 2.

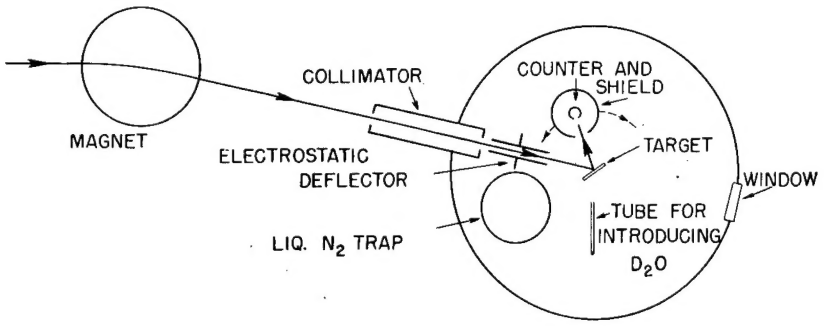

Figure 7. Experimental arrangement (diagrammatic).

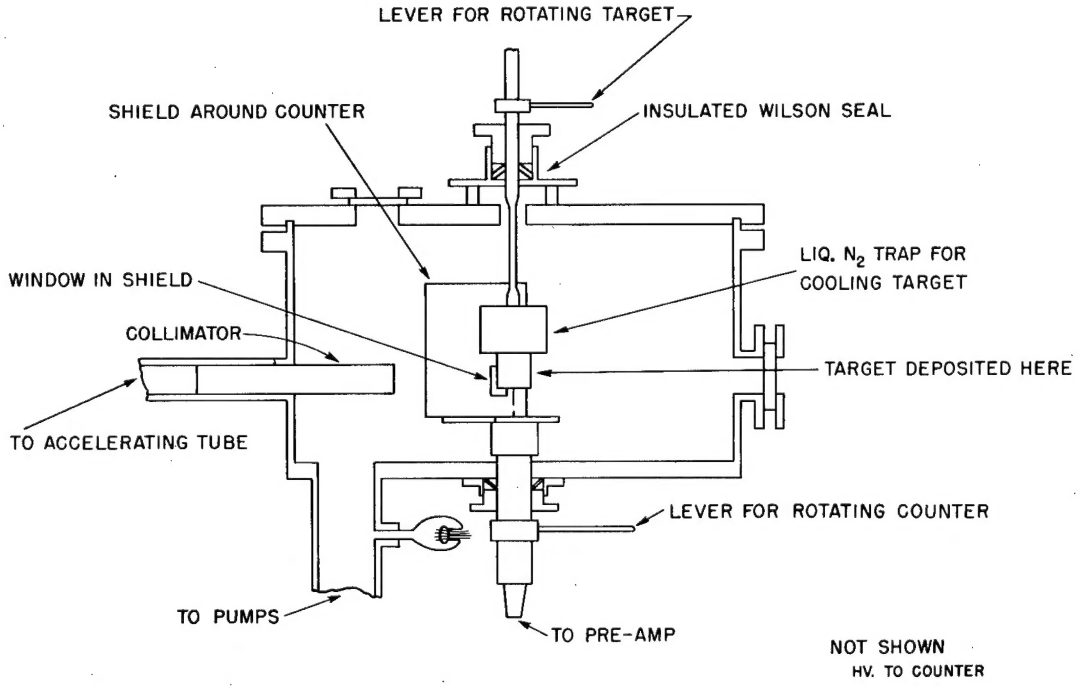

Figure 8. Vacuum tank (sectional view).

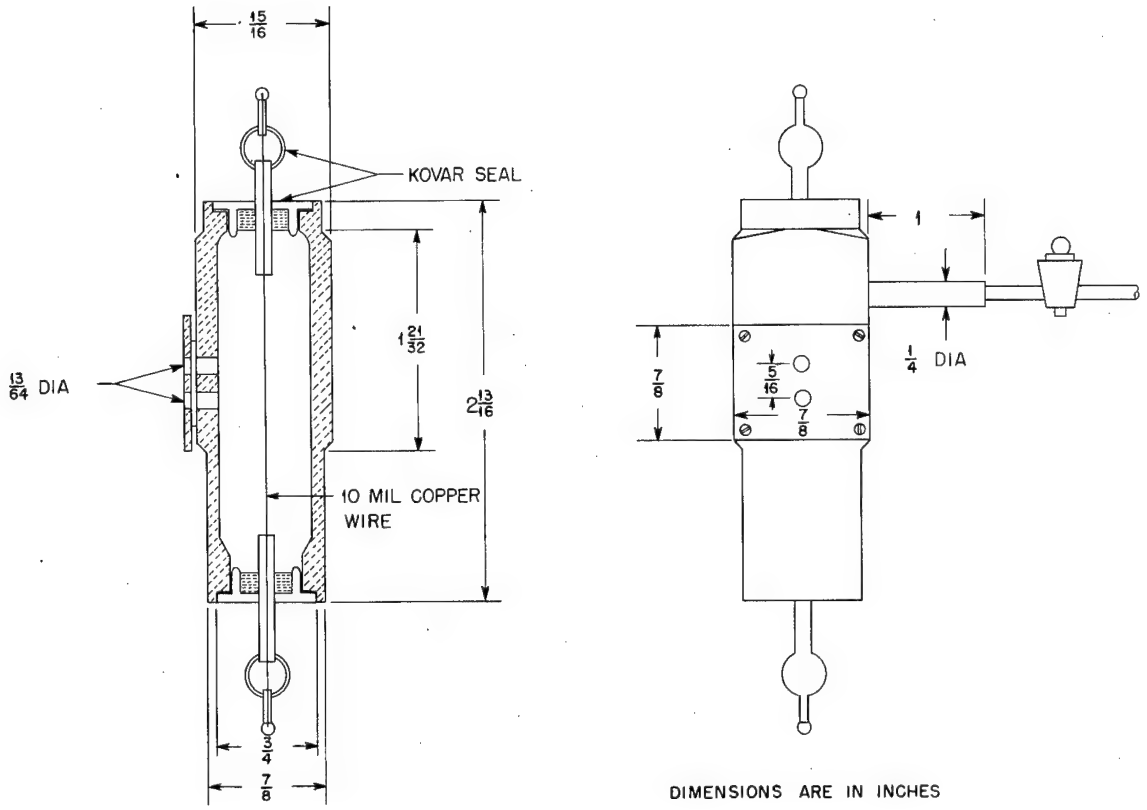

Figure 9. Counter used for excitation function and for angular distribution with good geometry.

(e) Voltmeters

An accurate measurement of the bombarding voltage was essential. To illustrate this, it may be pointed out that a change of incident deuteron energy of 1 Kev at 20 Kev produces a 30% change of reaction yield. Care was therefore taken to measure the bombarding voltage to ± 1%.

On the 15- to 50-Kev set, a 1-milliamp meter was put in series with two 20-megohm precision resistors. A further 10 megohms was later added in extending the measurements up to the full 50 Kev (Fig. 1).

For the 50- to 125-Kv set, a stack of 300 1-megohm precision resistors was made, and was used as a potential divider. The voltage across the bottom 1 megohm was applied to a circuit consisting of 16.5 megohms of precision resistors in series with a 30-microamp meter (Fig. 3). The ratio of the arms of the potential divider was measured using a Wheatstone bridge arrangement, and was found to vary by less than 0.3% under full load.

Both the 1-milliamp and the 30-microamp meter were separately calibrated; the deviation from the rated sensitivity was less than 1%.

(f) Other equipment

(i) A block diagram of the proton counting system is shown in Fig. 12. To reduce ripple and stray disturbances to a minimum, the high-voltage supply for the counter was from batteries in a shielded box, and the heater supply for the tubes of the preamplifier was rectified.

(ii) Besides the large auxiliary cooling trap in the tank, other traps were mounted immediately above the diffusion pumps.

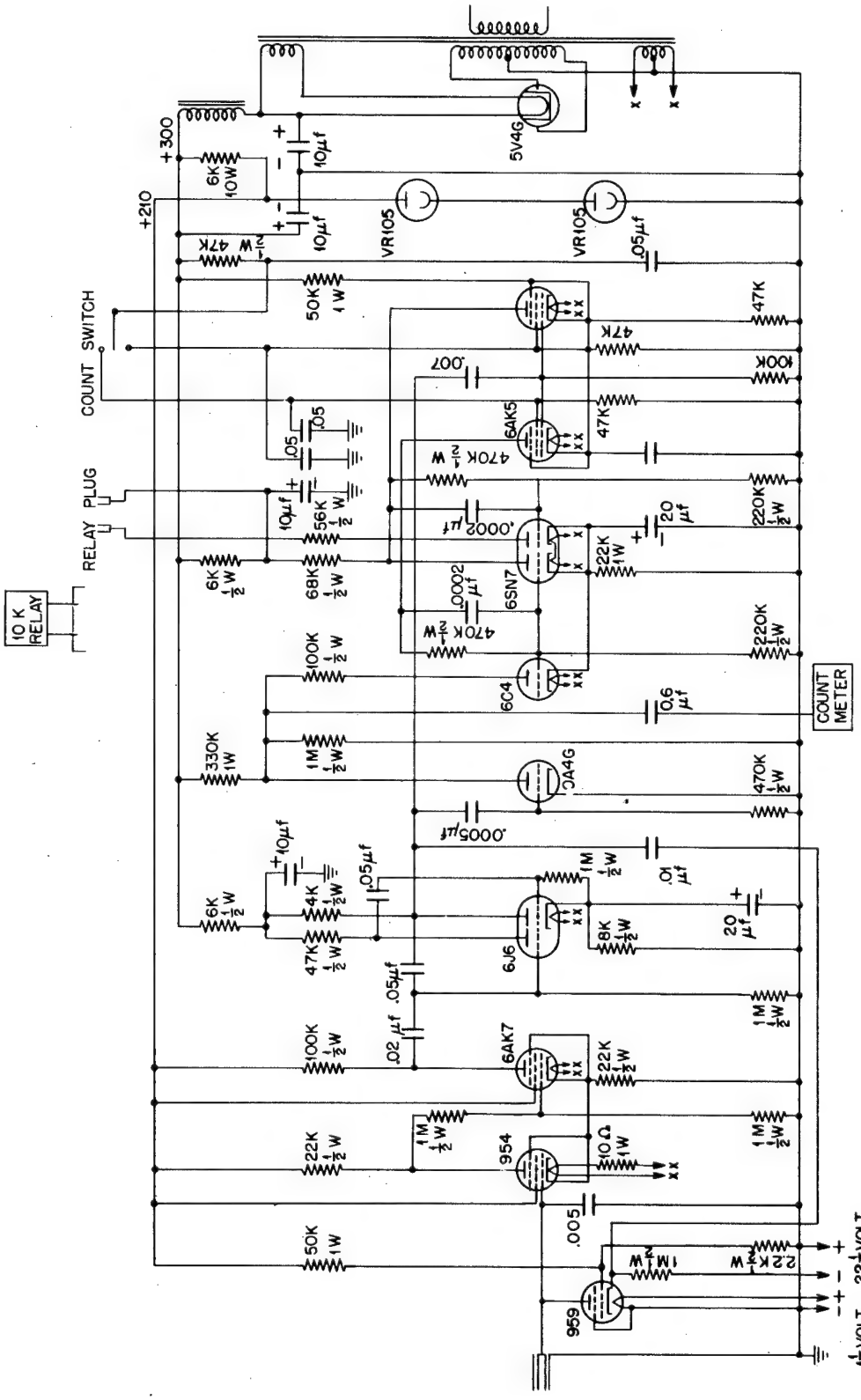

Figure 10. Automatic current integrator.

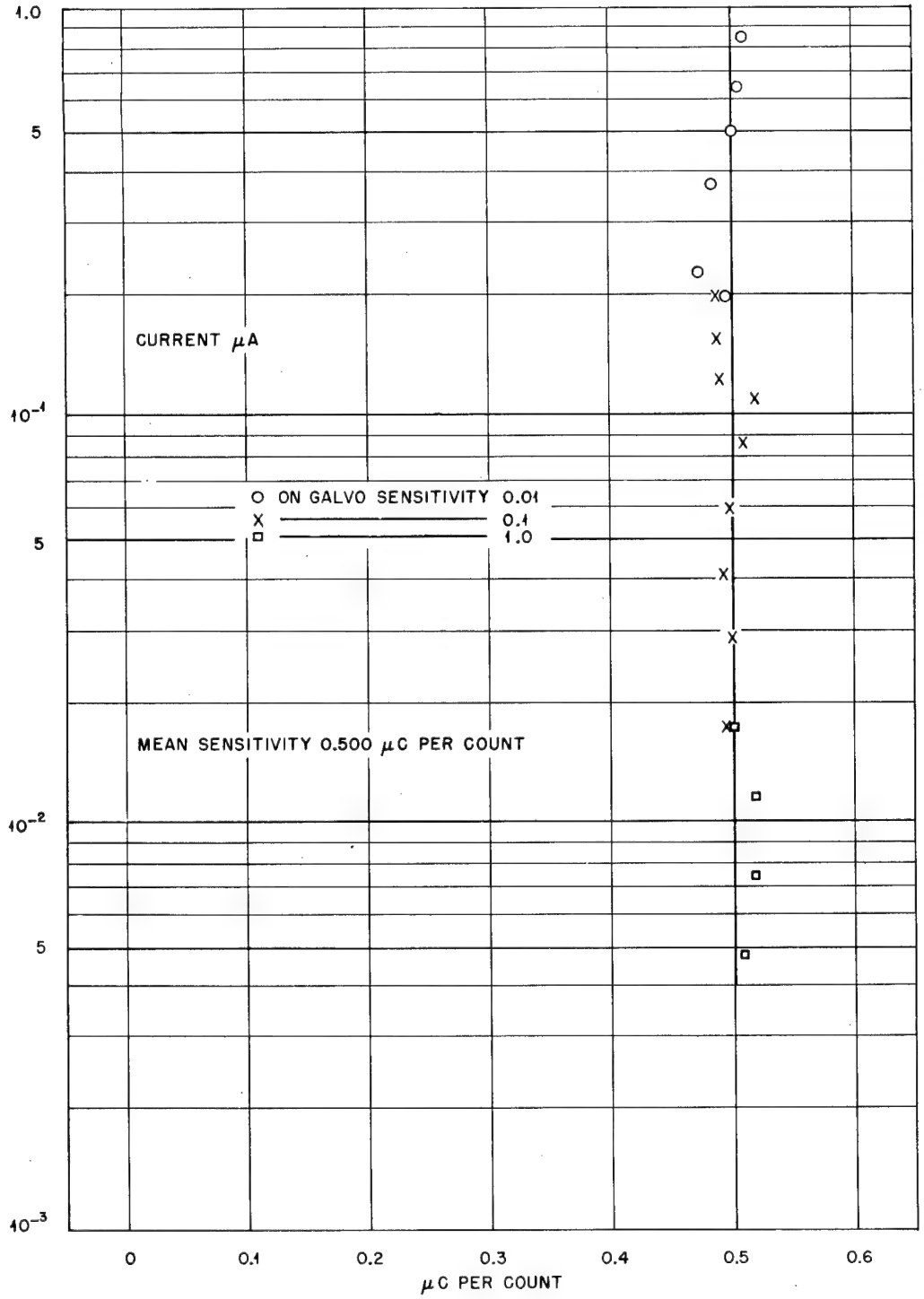

Figure 11. Current integrator sensitivity.

(iii) The deuterium gas was admitted to the ion source through a needle valve. The control was quite sensitive. The normal gas consumption was about 10 cc per hour, producing a pressure of about 5.10^{-5} mm in the accelerating tube.

Special Considerations

(a) Neutralization of the Beam

At low energies a beam of charged particles tends to suffer neutralization, and unless the pressure in the system is very low the effect may become serious. Since in these experiments the number of deuterons reaching the target was measured in terms of the positive charge collected, it was of the utmost importance to reduce neutralization to negligible proportions.

The essential step was to achieve as low a pressure as possible between the magnetic analyzer and the target, so that once a beam of charged particles of given velocity had been selected, it remained charged. The means of doing this has been described; it consisted simply in pumping the region from both ends. The pressure in the tank itself during a run was about 2.10^{-6} mm. There was probably a rise of pressure towards the magnet box, because of the low pumping speed of the beam collimator and the connecting tubes between tank and magnet box. But it is tolerably certain that the pressure everywhere in this region was below 10^{-5} mm.

To test the effectiveness of the system, the electrostatic deflector (Fig. 7) was used. With a deuteron beam of 17-Kev energy (one of the lowest energies employed) the disintegration yield was measured for the total beam and for that part of it which was not deflected away from the target by the electrostatic field. The conclusion was that only about 1.5% of the beam was neutralized. At higher energies the neutralization would of course be less, and no correction has been thought necessary for the effect.

(b) Target Contamination

It is well known that targets are easily contaminated. Traces of oil in the vacuum system become attached to the surface and are carbonized through the action of the beam. In particular, the effect is very marked in the case of a target cooled with liquid nitrogen, since any molecule striking the surface is likely to stick. If a vapour of molecular weight M is present at a pressure p in the system, the mass m of matter striking the target is given by:

$$M \sim pM^{\frac{1}{2}} \times 1.44.10^{-2} \text{ micrograms/cm}^2\text{/sec}$$
$$\sim pM^{\frac{1}{2}} \times 5.2.10^{-2} \text{ milligrams/cm}^2\text{/hr}$$

where p is measured in units of 10^{-6} mm. For a typical pump oil, p' is about 400. The range of the lowest-energy deuterons employed in the experiments was equivalent to a layer of about 15 micrograms per cm^2 of oil. At a pressure of 10^{-6} mm. such a layer would build up in approximately one minute. The need for extreme cleanliness in the vacuum system was thus apparent.

To achieve sufficiently good conditions for a run, the three auxiliary cooling traps were kept filled for several hours before the target trap itself was cooled. By this means, almost all condensible material was removed.

To investigate any possible target contamination which might still occur, two checks were possible. The first of these consisted in observing the change with time of the reaction yield for a given bombarding voltage. A specimen curve, for one of the lower bombarding voltages (where the effect is most serious) is shown in Fig. 13. The errors shown for individual points are statistical. The second method was to measure the yield, for a given bombarding voltage, as a function of the angle ϕ between the face of the target. If an oil film existed, its thickness in the direction of the deuteron beam would vary as cosec ϕ, and the yield would be changed. Fig. 14 shows the result of this test for 40 Kev bombarding energy.

In the light of these observations it was considered that the contamination problem had been adequately dealt with .

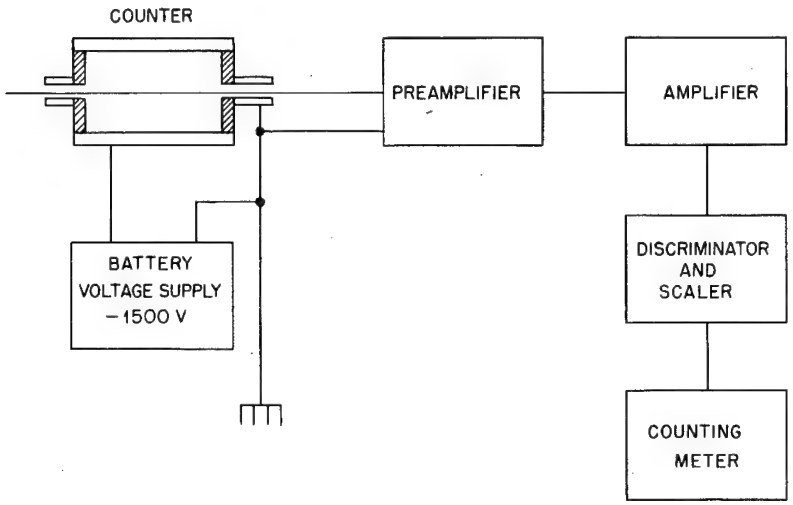

Figure 12. Counting system.

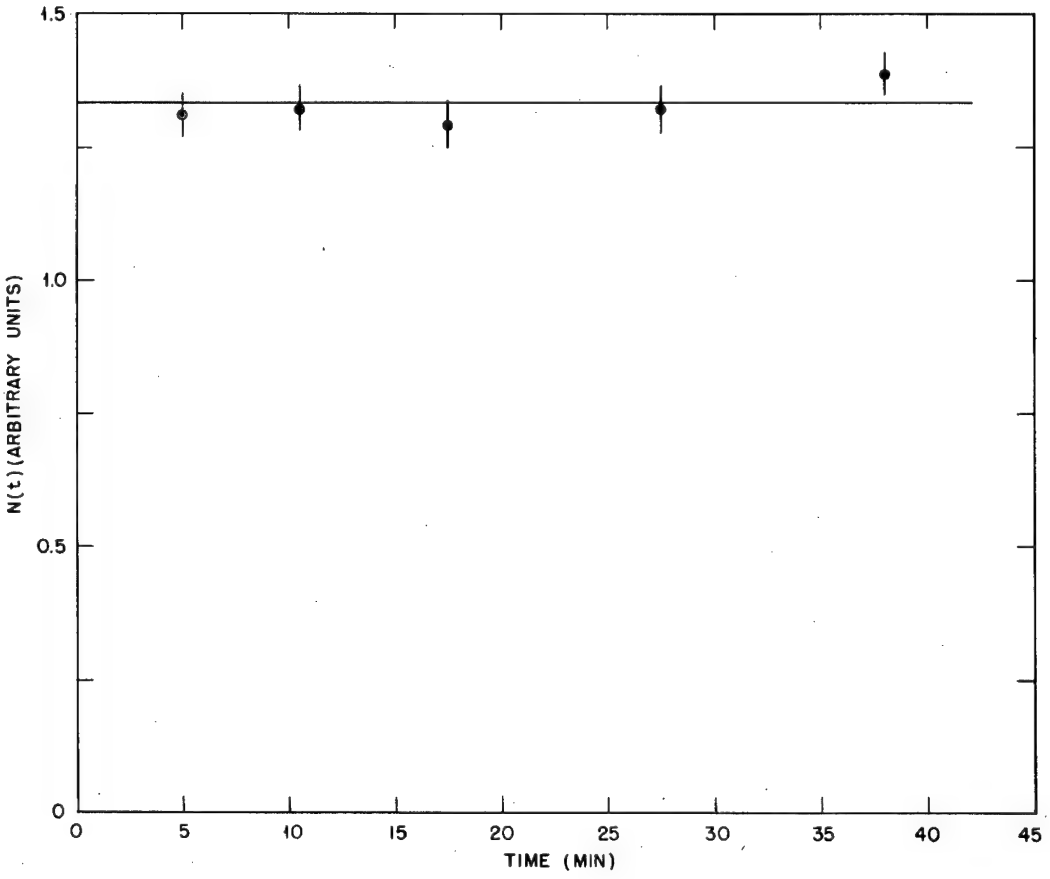

Figure 13. Change of yield with time, deuteron energy = 20 kev.

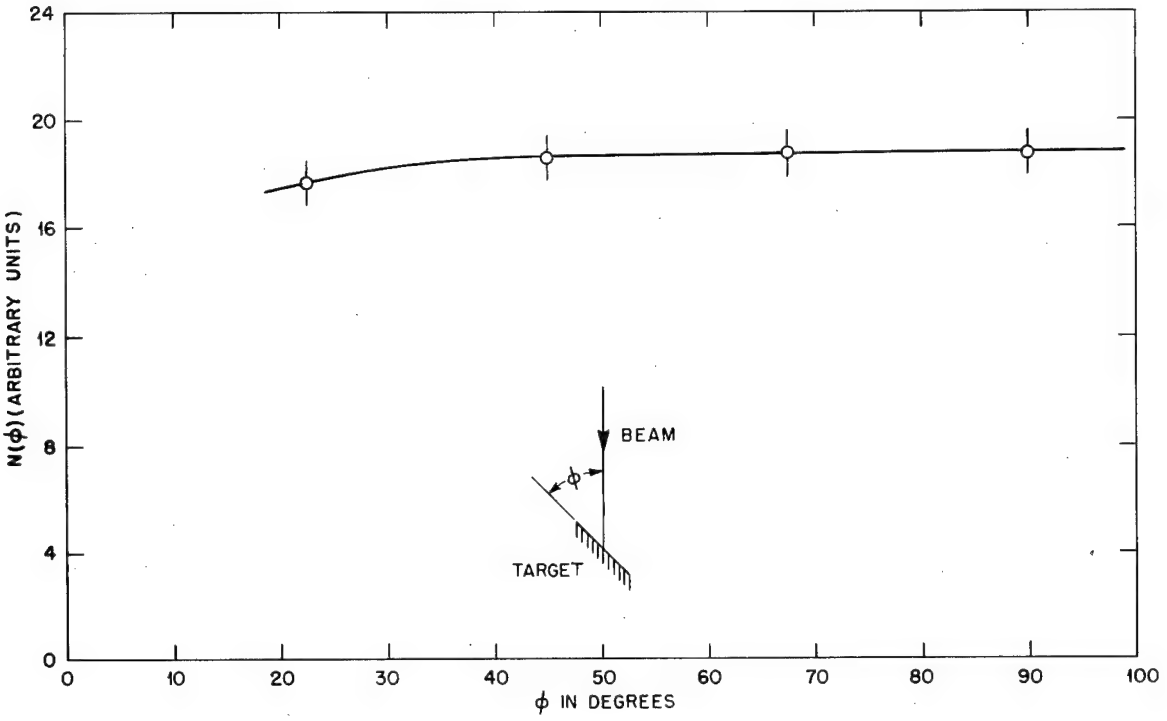

Figure 14. Apparent yield per μc vs. target setting, deuteron energy = 40 kev.

(c) Secondary Electron Emission

In measuring the beam current in experiments of this type, it is always a matter of some concern to know whether the recorded target current corresponds to the true current of positive ions reaching the target. Secondary electrons, often several per deuteron, are liberated at the target and any other point where the beam may strike. For a deuteron beam of 100 Kev, the maximum possible secondary electron energy is about 100 ev, and the majority of electrons have much lower energies than this. Consequently, a positive voltage of about 100v on the target was sufficient in this work to ensure effectively no escape of secondaries from the target itself. There remained the problem that this potential might collect a few secondaries produced at the second slit of the beam collimator (see Fig. 7).

To test whether this was so, a cylindrical permanent magnet was mounted surrounding the collimator, with its axis along the axis of the beam.

It was magnetised to give a field whose component transverse to the axis had a value of about 20 gauss at the collimator slit. This field, combined with the electrostatic field due to the positive voltage on the target, sufficed to make the electrons follow spiral paths towards the tank walls, without appreciably affecting the deuterons. The chance of an electron encountering the target was then small. The thick target reaction yield, per microcoulomb of effective beam current, was found to be the same before and after insertion of the magnet.

A later test, on the variation with positive target voltage of the reaction yield per microcoulomb of measured beam, gave the result shown in Fig. 15.

On the basis of this evidence, it is thought that the measurement of beam currents was satisfactory.

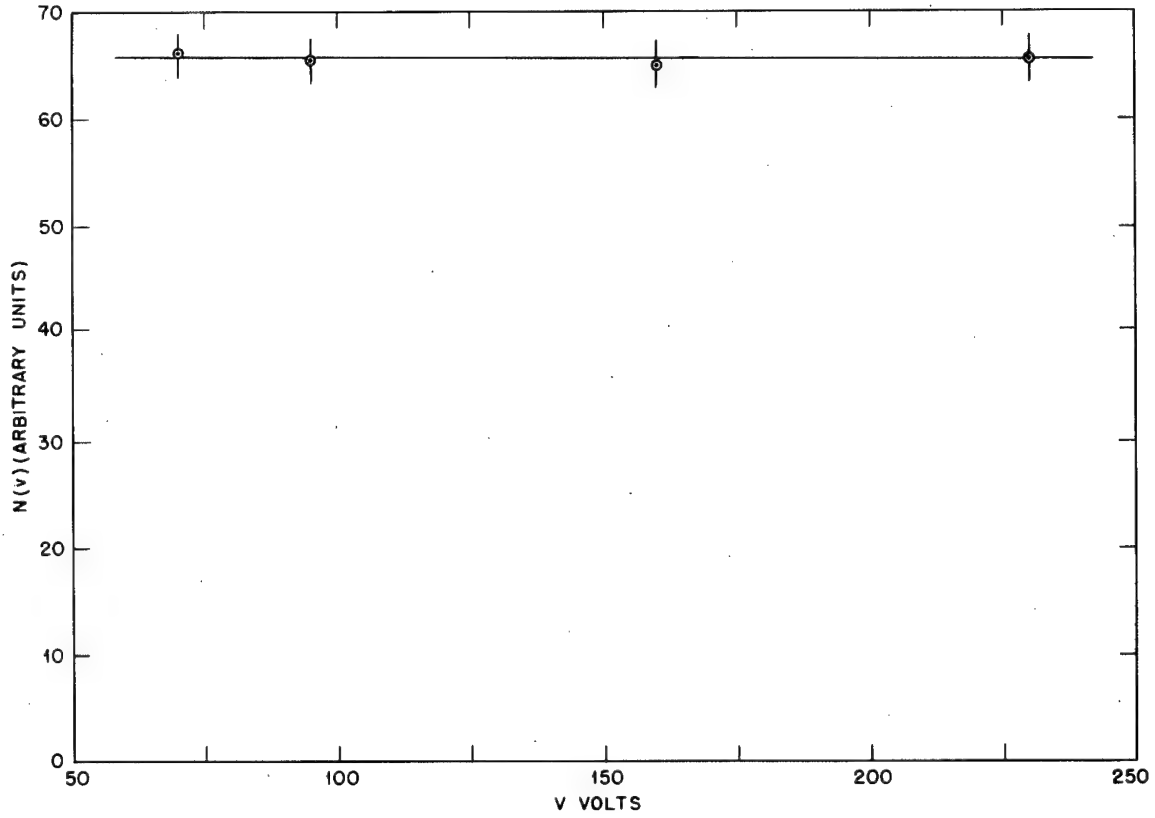

Figure 15. Apparent yield per μc vs. positive target voltage, deuteron energy = 80 kev.

The Determination of N(E).

Let the fraction of 4π subtended by the counter window at the target spot be denoted by F, and let $n(\theta)$ be the number of protons per microcoulomb of beam observed in the counter at setting θ, for some particular bombarding energy E. Then evidently,

$$N(E) = \frac{1}{2F} \int_0^{\pi} n(\theta) \sin \theta . d\theta \qquad (1)$$

That is, the total yield at E can be found by observing $n(\theta)$ for all values of θ from 0 to π and numerically integrating the result.

Although this is perfectly feasible, it is also tedious, and a simpler alternative method was adopted: Let $n'(\theta')$ be the hypothetical count at an angle θ' in the center-of-gravity system corresponding to the observed count $n(\theta)$ in the laboratory system. Then:

$$N(E) = \frac{1}{2F} \int_0^{\pi} n(\theta).\sin\theta.d\theta = \frac{1}{2F} \int_0^{\pi} n'(\theta').\sin\theta'.d\theta' \qquad (2)$$

Thus, $$n(\theta) \sin\theta \, d\theta = n'(\theta')\sin\theta'.d\theta'$$

or $$n'(\theta') = n(\theta).g(\theta) \qquad (3)$$

where $$g(\theta) = \frac{d(\cos\theta)}{d(\cos\theta')}$$

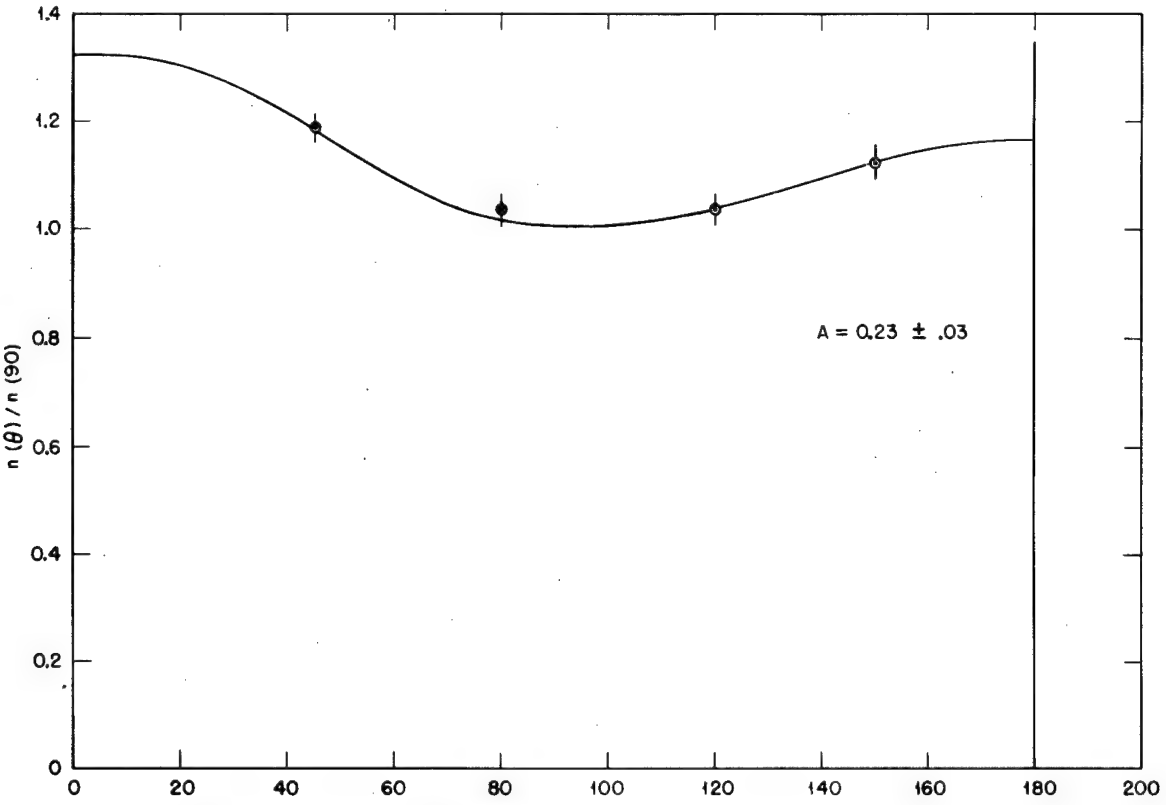

Figure 16. Angular distribution D + D 20 kev. Laboratory system.

$g(\theta)$ and $(\theta' - \theta)$ can be readily evaluated from the bombarding energy E and the heat of reaction Q (see appendix). Although, strictly speaking, $g(\theta)$ refers to a single value of E, a weighted mean value corresponding to a thick target, where all values of bombarding energy from 0 to E come into play, can be arrived at from an approximate knowledge of the excitation curve. Thus $n'(\theta')$ can be found from an observation of $n(\theta)$.

Now for the D + D reaction, the angular distribution in the center-of-gravity system can be closely represented by:

$$n'(\theta') = n'(90°)\left[1 + a(E)\cos^2\theta'\right] \tag{4}$$

a (E) is the 'asymmetry coefficient', and refers to a thin-target yield at a single energy. For a thick-target yield, a similar formula holds, but a (E) is replaced by a smaller quantity A(E), since the angular distribution becomes less anisotropic at low energies. Thus one has:

$$N'(\theta') = n'(90°)\left[1 + A(E)\cos^2\theta'\right] \tag{5}$$

and this equation can be used to represent observations on thick-target yields, provided that E is not too large. (This limitation arises because various angles $\theta(E)$ in the laboratory contribute to a single value of θ' in the center-of-gravity system). Integrating equation (5), one obtains N(E) (cf. equation (2)). The result is:

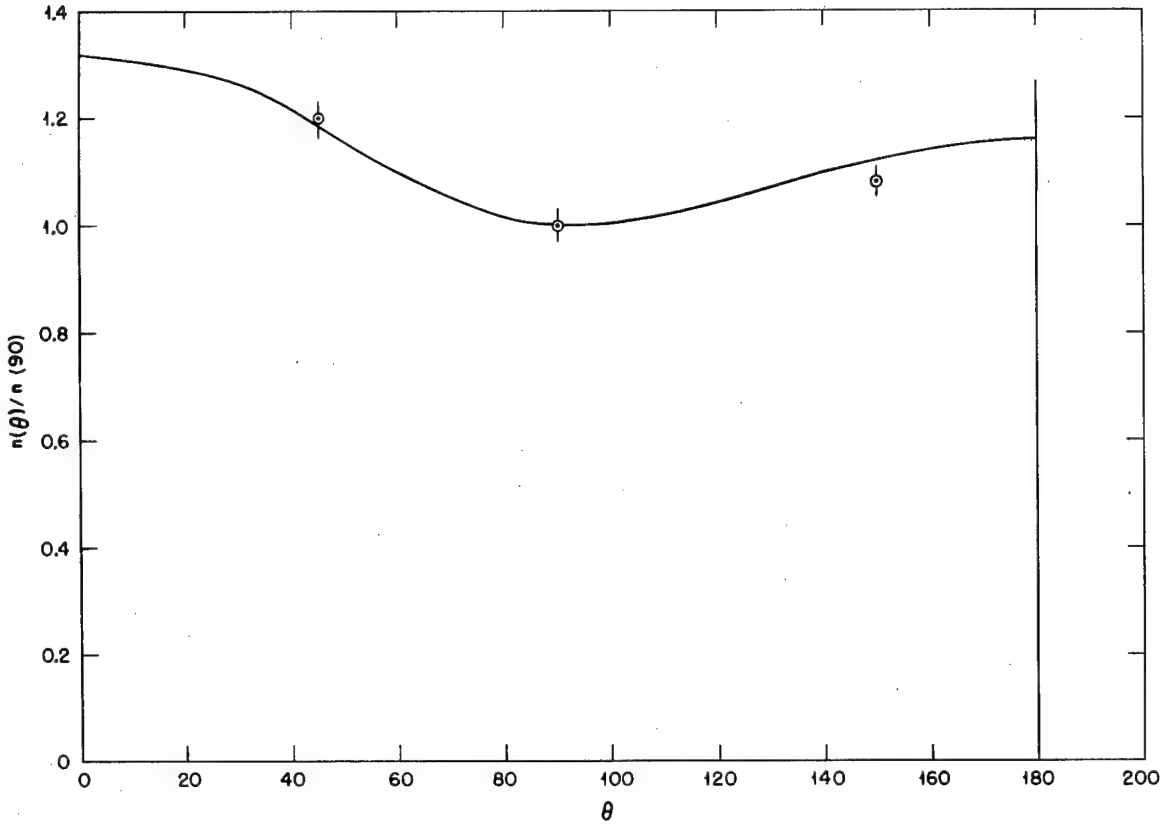

Figure 17. Angular distribution D + D 30 kev. Laboratory system.

$$N(E) = \frac{1}{2F} \cdot n'(90°)\left[2 + \frac{2}{3}A(E)\right] = \frac{1}{F} \cdot n'(90°)\left[1 + \frac{1}{3}A(E)\right] \tag{6}$$

If observations are made at a particular angle θ_0 in the laboratory system, corresponding to θ'_0 in the center-of-gravity, then:

$$N(E) = \frac{1}{F}\, n'(\theta'_0)\, \frac{1 + \frac{1}{3}A(E)}{1 + A(E)\cos^2\theta'_0} \tag{7}$$

as follows from equation (5). Now if in particular θ'_0 is chosen so that:

$$\cos^2 \theta'_0 = \frac{1}{3} \tag{8}$$

then equation (7) reduces simply to:

$$N(E) = \frac{1}{F}\, .n'(\theta'_0) \tag{9}$$

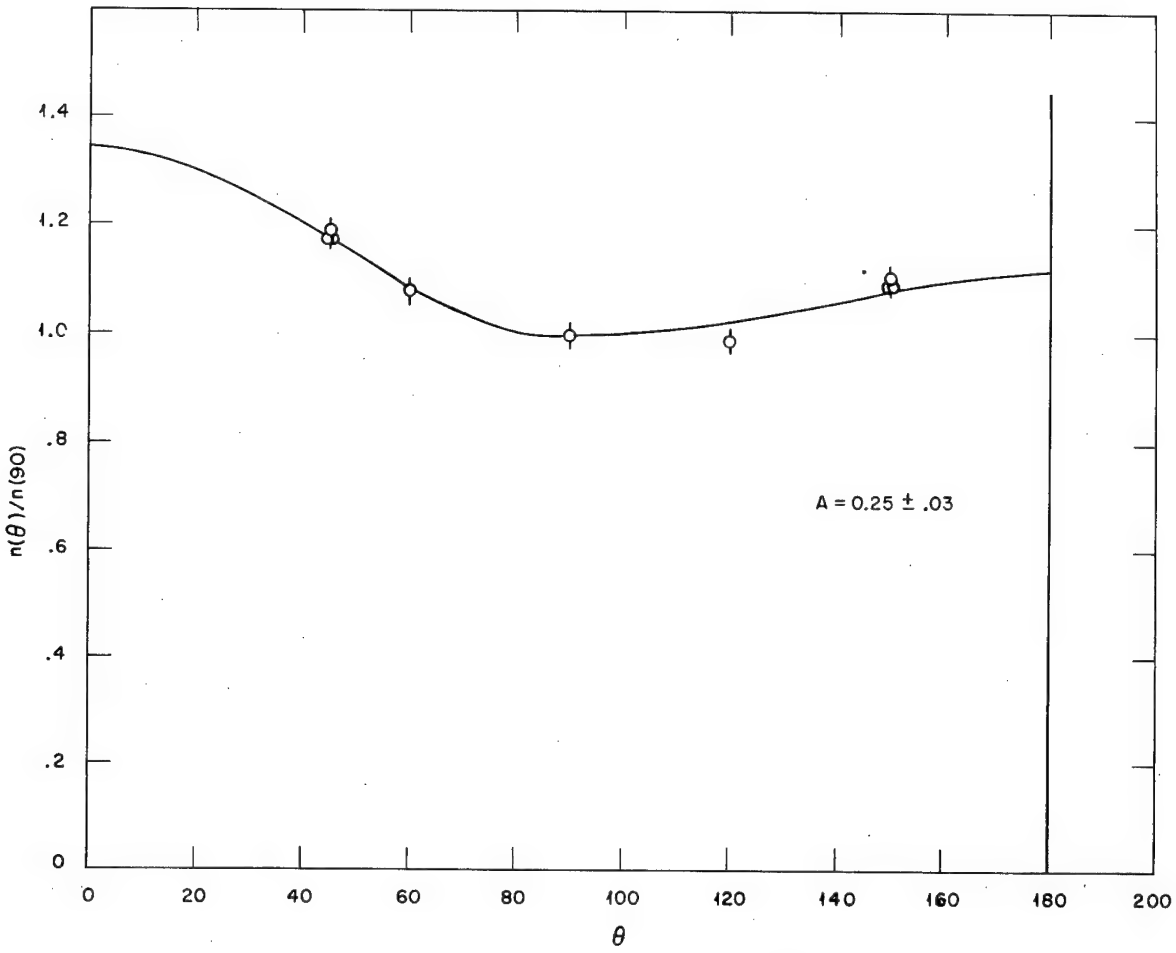

Figure 18. Angular distribution D + D 40 kev. Laboratory system.

That is, the total yield can be found from observations at a single angle, without a knowledge of the asymmetry coefficient A(E). The only condition for this to be true is that equation (5) should be obeyed.

Equation (8) is fulfilled for $\theta_0' = 54°44'$ or $125°16'$. The corresponding angles θ_0 in the laboratory system vary of course with E, but, for E = 125 kev, are different only about 3° from the angles in the center-of-gravity.

If observations are made at angles 54°44′ or 125°16′ in the laboratory system, the errors thereby introduced, for a maximum bombarding energy of 105 kev, are -2.5% and +1.5%, respectively (see Appendix). Because of the smaller error at the backward angle, observations were always taken with this counter setting (of 125° in the laboratory), and it could be safely assumed that the total thick-target yield was given, with an error of less than 2%, by the equation:

$$N(E) = \frac{1}{F}\, g(\theta_0)\, n(\theta_0) \qquad (10)$$

in which $\theta_0 = 125°$.

The first step in applying this method was to establish the validity of equation (5), and measurements on the angular distribution were made at a series of energies. Such a detailed study was not really demanded for the purpose of this experiment, but a knowledge of a(E) as a function of E, derived from the observed values of A(E), was of interest to the theoreticians. With its aid, certain deductions

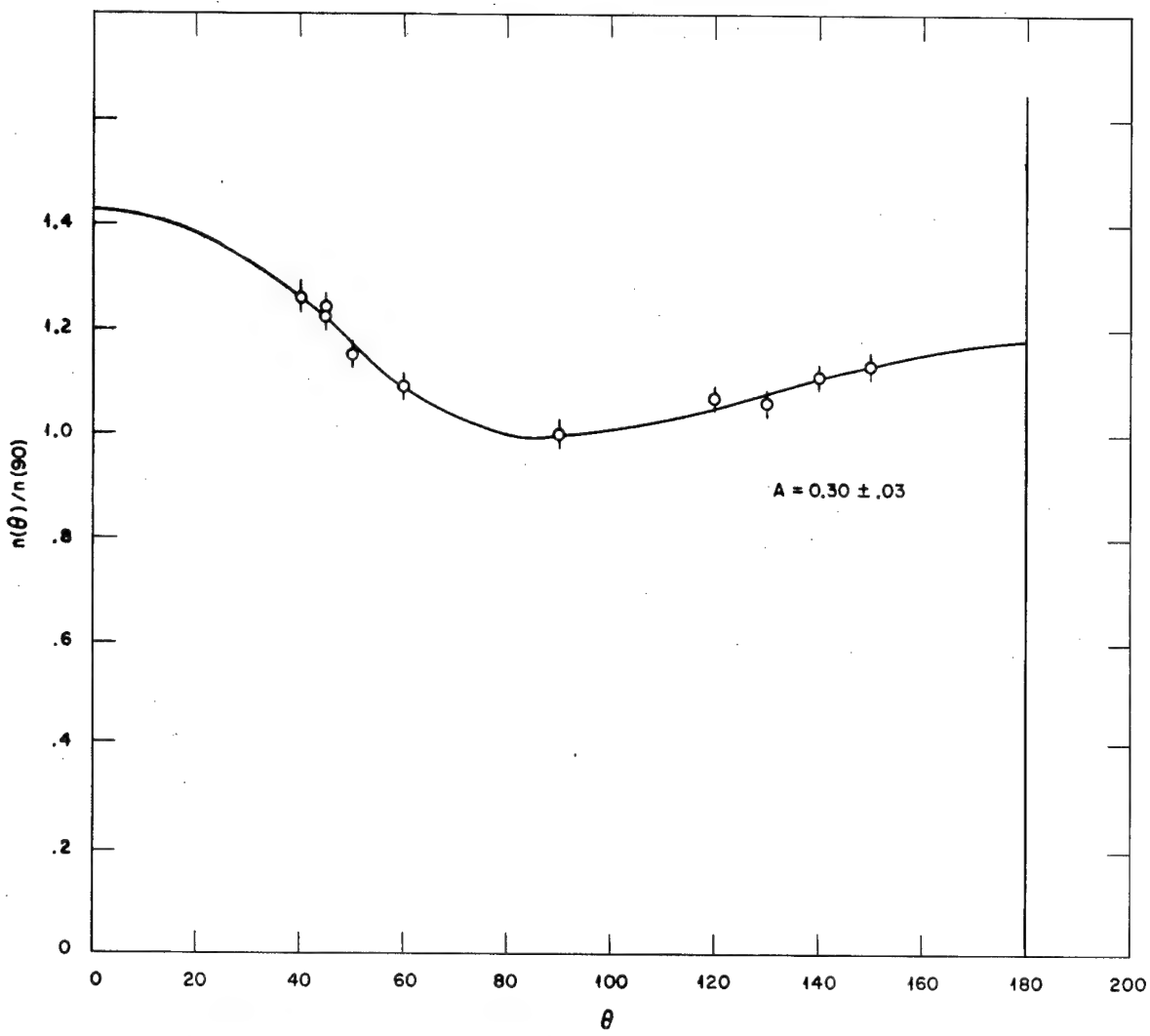

Figure 19. Angular distribution D + D 50 kev. Laboratory system.

could be made concerning the nuclear radius of the deuteron and the precise nature of the D-D interaction (see E. J. Konopinski: Technical Series, Vol 3, ch. 7).

The means of deriving a(E) from A(E) is given in the Appendix.

Results of Angular Distribution Measurements

In Figures 16 to 20 are shown the experimental results of the angular distribution measurements. In each case a full curve has been drawn through the experimental points, corresponding to the theoretical relations:

$$\left.\begin{aligned} n'(\theta') &= n'(90°)\ \left[1 + A(E)\cos^2\theta'\right] \\ n'(\theta') &= g(\theta)\ .n(\theta) \end{aligned}\right\} \text{evaluated with that value of A(E)}$$

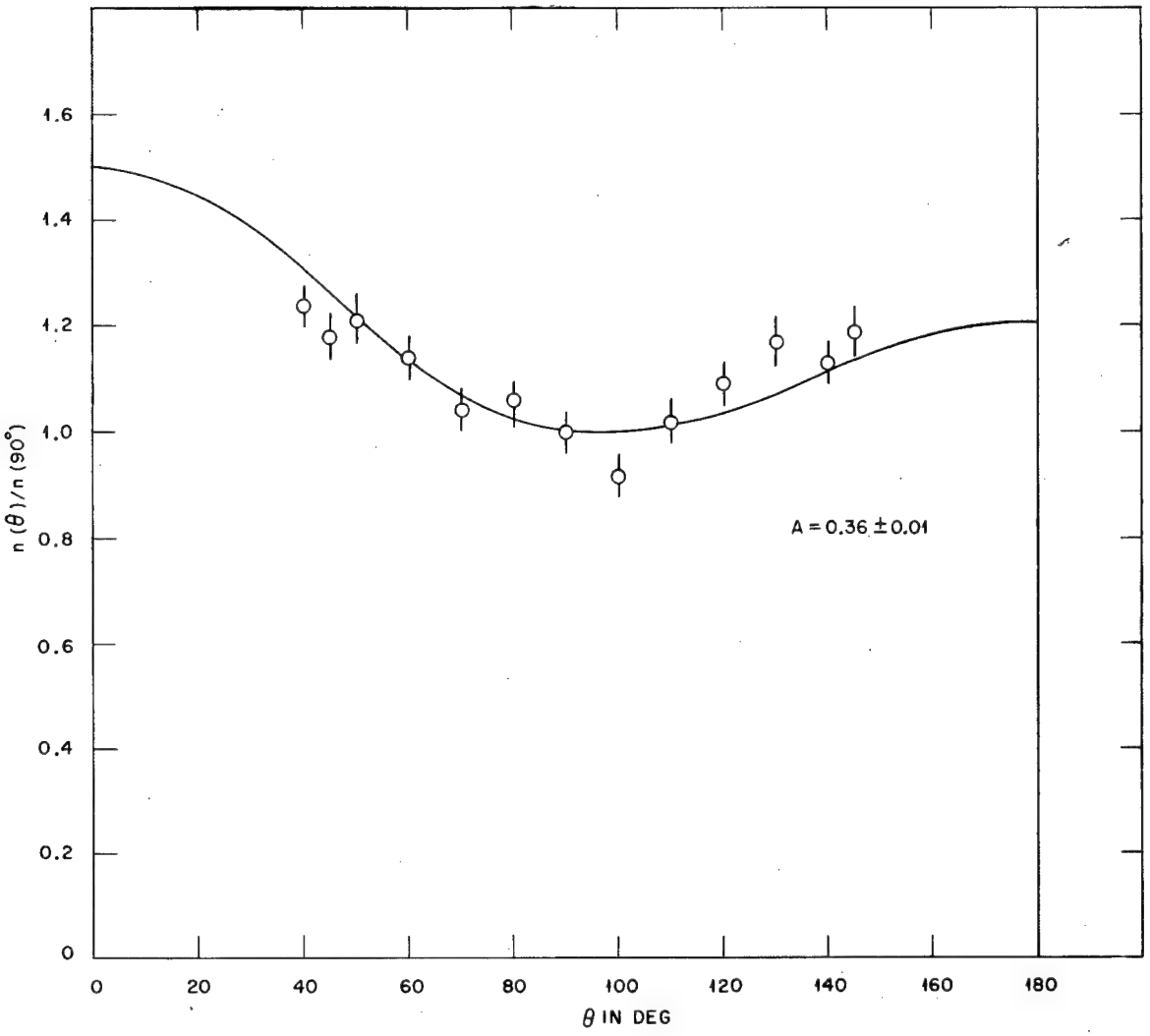

Figure 20. Angular distribution D + D 79 kev.

which best fits the data. It may be seen that the agreement between theory and experiment is quite good. A more exacting test of the results consists in plotting the quantity $\left[\frac{n'(\theta')}{n'(90°)} - 1\right]$ against $\cos^2\theta'$. Since the degree of anisotropy is small, any experimental errors become greatly magnified. A plot of this kind is shown in Figures 21 and 22 for bombarding energies of 50 kev and 79 kev, respectively.

A(E) as a function of E is shown in Figure 23. The derived curve (see Appendix) representing a(E) vs. E is also given in this figure. It may be seen that the asymmetry coefficient shows no sign of tending to zero at zero bombarding energy. It has been thought convenient to use a linear relation to express the variation of A(E) and a(E) with energy, although it is clear that the results in themselves are not accurate enough either to justify or to vitiate this assumption.

It has been thought of interest to present the values of A(E), found from these experiments, on a graph which also contains the results obtained by Manley, Graves, et al (CF-1565) at somewhat higher energies. This is done in Figure 24.

The quantity $g(\theta)$, which is used so extensively in analyzing the results, both of the angular distribution and of the excitation curve measurements, is shown as function of energy and angle in Figure 25.

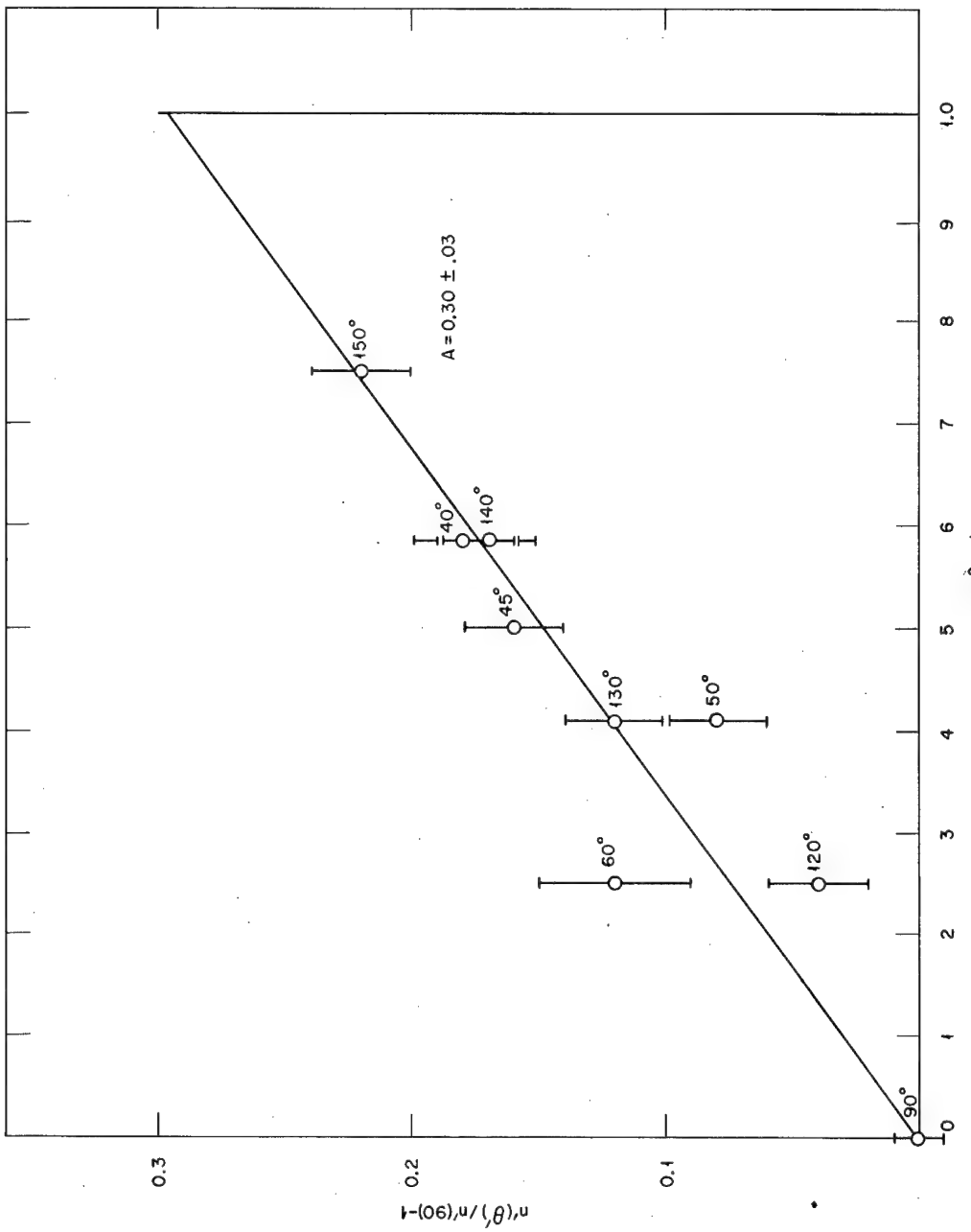

Figure 21. D + D 50 kev. Test of $\cos^2\theta'$ law. $\left[\frac{n'(\theta')}{n'(90)} - 1\right]$ vs. $\cos^2\theta'$, i.e., $A\cos^2\theta$ vs. $\cos^2\theta'$.

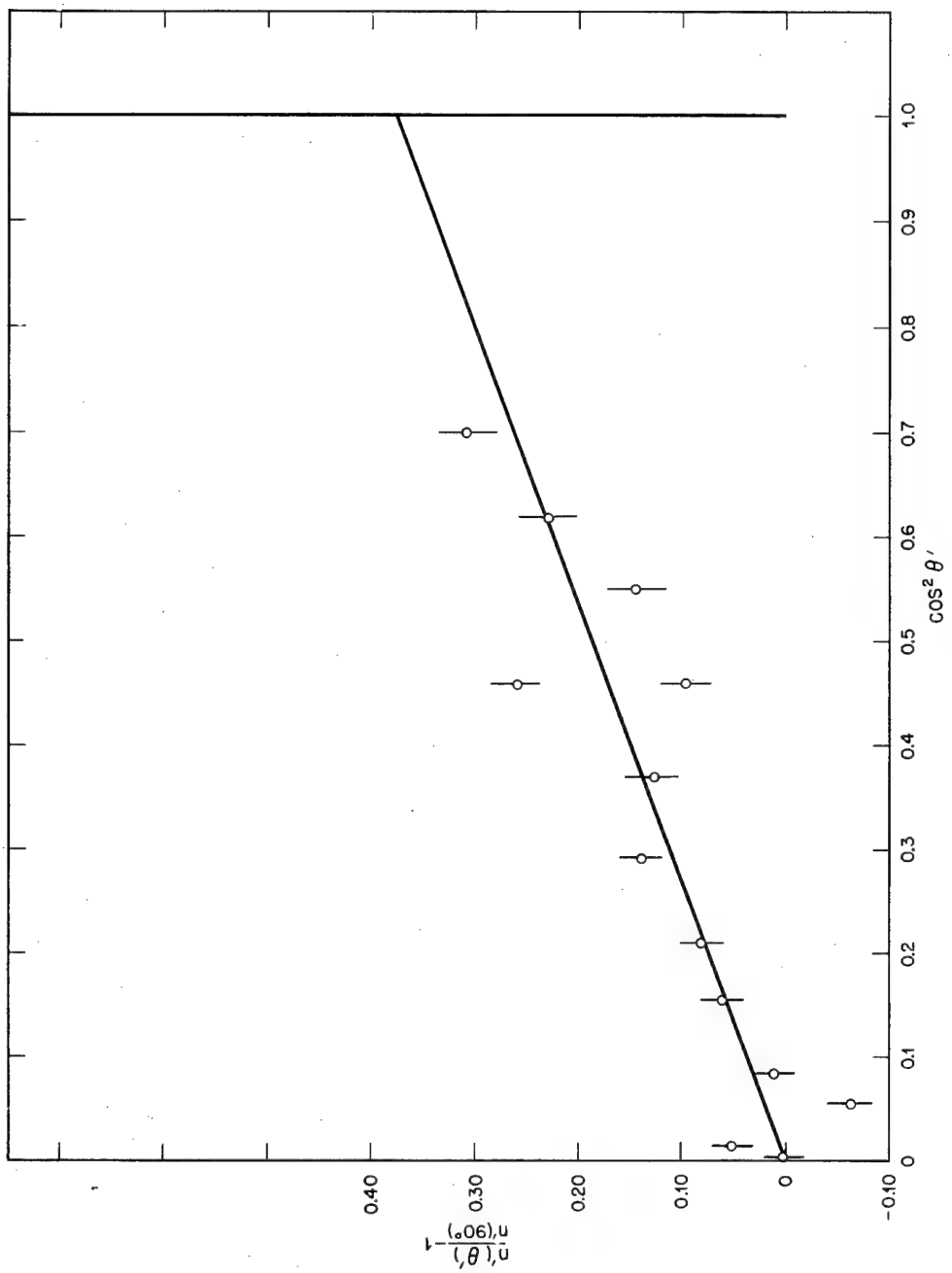

Figure 22. Test of $\cos^2\theta'$ law for D + D at 76 kev. $\left[\frac{n'(\theta')}{n'(90°)} - 1\right]$ vs. $\cos^2\theta'$, i.e., A $\cos^2\theta'$ vs. $\cos^2\theta'$.

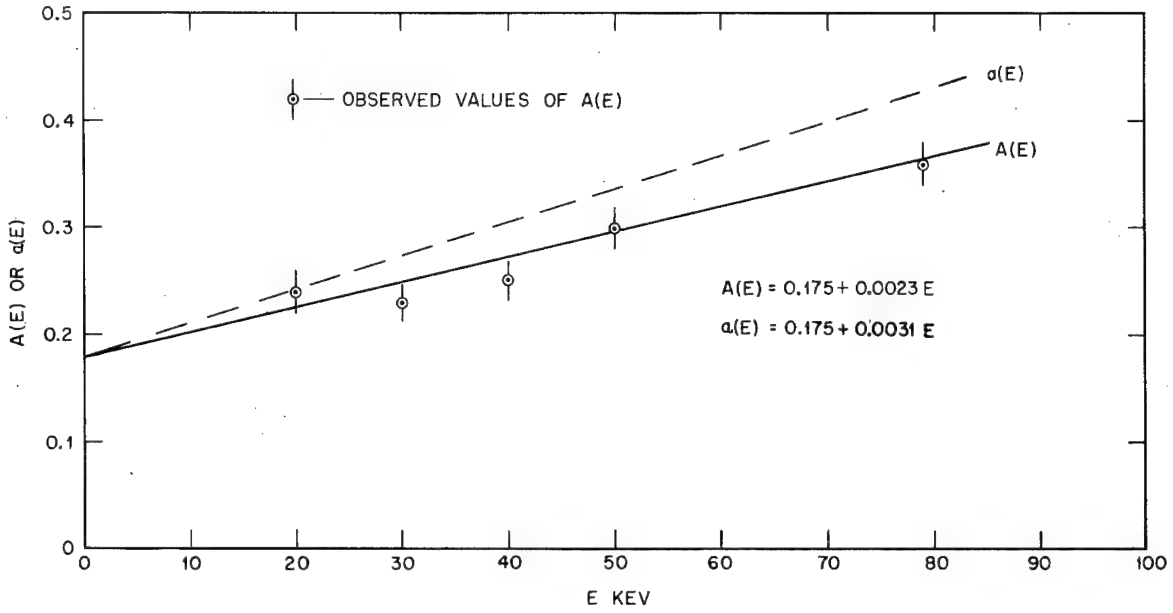

Figure 23. A(E) & a(E) vs. E.

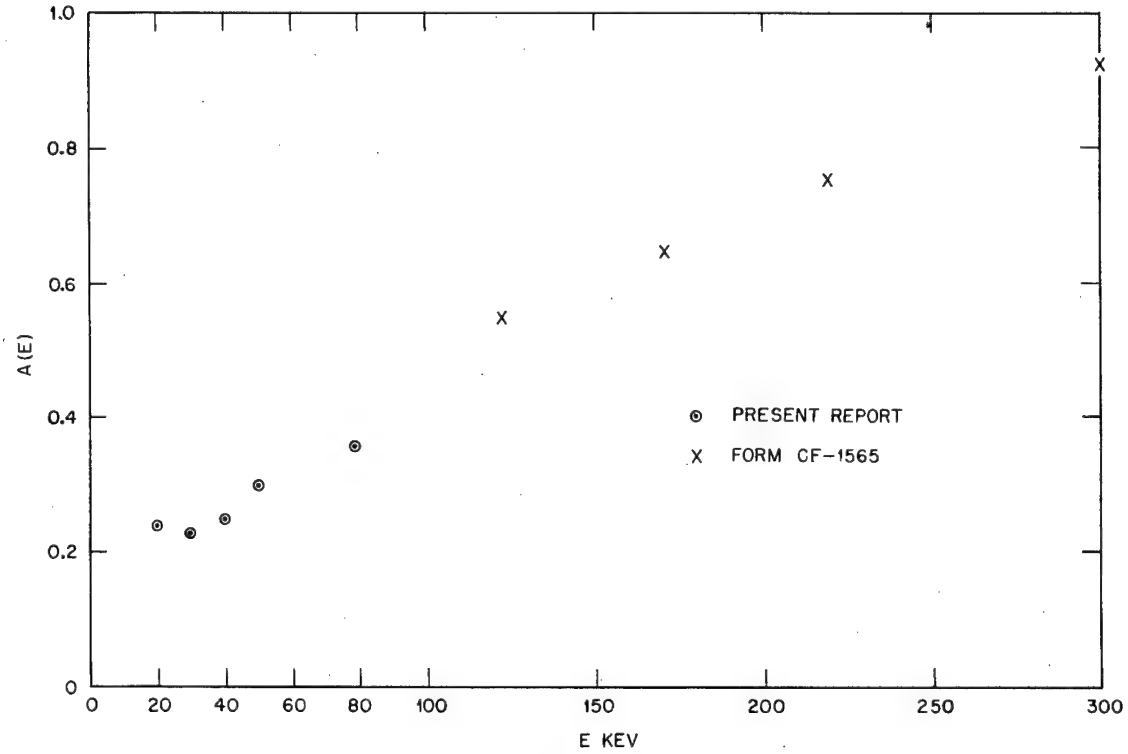

Figure 24. A(E) vs. E, 20 kev.–300 kev.

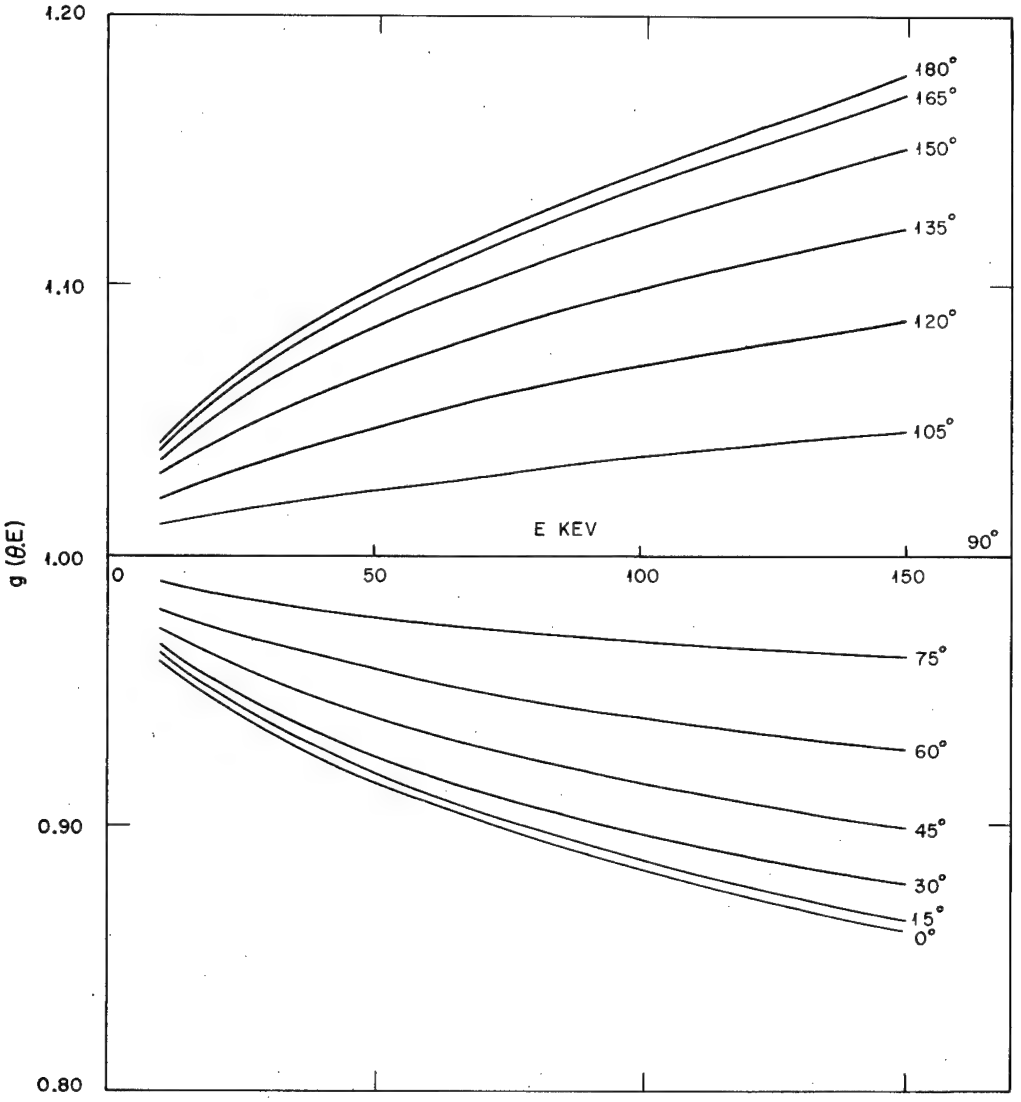

Figure 25. g(θ) vs. E, D + D proton emission.

Excitation Curve Measurements

Observations on the thick-target yield as a function of energy were made using both mass-4 and mass-2 beams, with a counter setting of 125 throughout. The mass-4 beam was assumed to be pure D_2^+, so that a measurement of the yield per microcoulomb of target current led directly to a knowledge of the number of protons per incident deuteron produced by the nuclear reaction. With this beam, however, deuterons of only half the maximum bombarding energy could be obtained. Through the employment of the mass-2 beam, containing D_1^+ ions, the full bombarding voltage could be utilized, but there was in this case the disadvantage that the mass-2 beam contained some H_2 as well as D_1^+. Thus the measured yield per unit of beam current was lower than the true yield per microcoulomb of deuterons. To correct the apparent mass-2 yields to true values, the following method was adopted:

A 'Gamow' plot was made of log N(E) vs. $E^{-\frac{1}{2}}$. In this representation the yield curve becomes essentially a straight line. The lines corresponding to mass-4 and mass-2 (apparent) yields were parallel, showing that the H_2^+ content of the mass-2 beam was independent of energy. The distance between the lines determined the constant factor by which the observed mass-2 yields were to be increased to give the true values. The actual results are shown in Figures 26 and 27 for the low-energy and high-energy measurements, respectively. It may be seen that the correction factor for mass-2 beam impurity is readily determined by this means, and, since it makes use of all the observations, is probably more reliable than a single comparison of the yields for mass-2 and mass-4 beams having the same deuteron velocity.

N(E) was then obtained from the corrected values of n(125°) with the aid of equation (10). F was known from careful measurements of the sizes of the counter windows and their distance from the target. The working is set out in Table 1 below. The complete excitation curve, for energies from 15 kev to 105 kev, is shown in Figure 28 as a Gamow plot, and log N(E) vs. E is given in Figure 29.

Table 1.

E	$E^{-\frac{1}{2}}$	n(125°)+	$\frac{1}{F}$, n(125°)*	g(125°)++	N(E)
15.4 kev	8.05 $(Mev)^{-\frac{1}{2}}$	0.240 counts	$2.47.10^2$	1.025	$2.53.10^2$
18.1	7.45	0.607 per	$6.24.10^2$	1.028	$6.40.10^2$
20.5	7.00	1.15 C.	$1.18.10^3$	1.030	$1.21.10^3$
23.0	6.60	2.23	$2.29.10^3$	1.031	$2.36.10^3$
23.8	6.47	2.64	$2.71.10^3$	1.032	$2.79.10^3$
26.4	6.15	3.42	$4.30.10^3$	1.033	$4.43.10^3$
30.6	5.67	8.37	$8.60.10^3$	1.035	$8.88.10^3$
31.6	5.60	7.90	$9.90.10^3$	1.037	$1.03.10^4$
35.6	5.25	16.8	$1.73.10^4$	1.040	$1.80.10^4$
39.6	5.02	18.5	$2.32.10^4$	1.042	$2.41.10^4$
40.9	4.92	27.3	$2.81.10^4$	1.044	$2.93.10^4$
45.6	4.68	40.2	$4.13.10^4$	1.046	$4.32.10^4$
47.7	4.56	47.7	$4.90.10^4$	1.047	$5.13.10^4$
52.8	4.35	50.0	$6.29.10^4$	1.050	$6.59.10^4$
63.2	3.97	88.0	$1.11.10^5$	1.055	$1.17.10^5$
79.2	3.56	174	$2.19.10^5$	1.061	$2.32.10^5$
95.0	3.25	286	$3.60.10^5$	1.070	$3.85.10^5$
105.6	3.08	354	$4.45.10^5$	1.075	$4.78.10^5$

+ Mass-2 yields already corrected for beam impurity.

++ Thick target values of g(125°).

*Note that two distinct values of F are used in forming these products; for the higher energy work it was somewhat smaller than for the low energy experiments. (cf. Figures 26 and 27).

Note on Errors

The counting error at the lowest energy employed was about 7%. For the majority of the measurements, however, it was not in excess of 1%. The bombarding energy was known within 1%. The beam current measurements with the integrator are probably good to ±2%. So far as could be discovered, any errors due to target contamination or secondary electron emission were together not more than 1%. The error due to observing at 125° in the laboratory system instead of 125° in the center-of-gravity system is always less than 1.5%. The error due to the presence of neutral particles

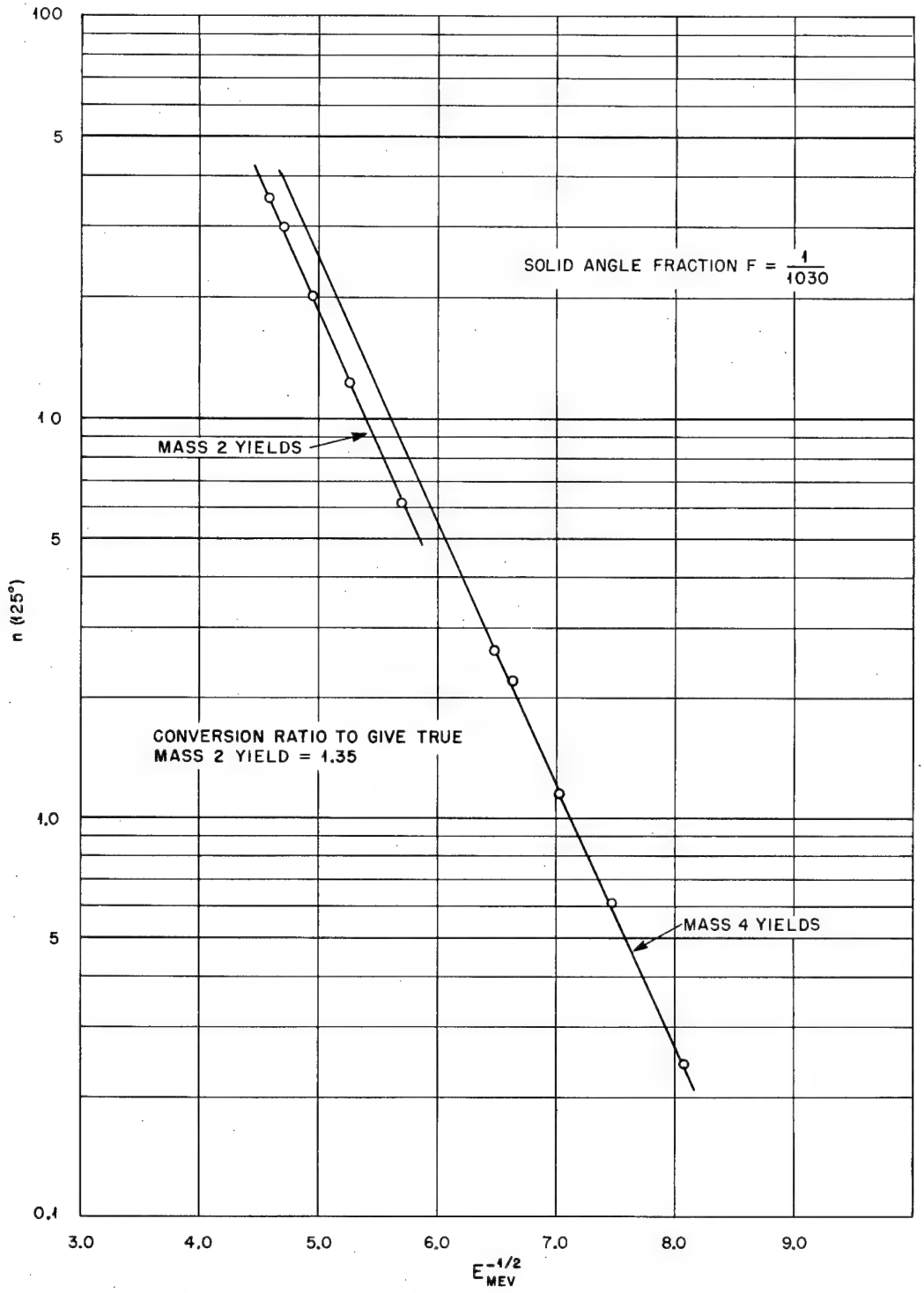

Figure 26. Excitation curve measurements at lower energies (15 kev−50 kev.)

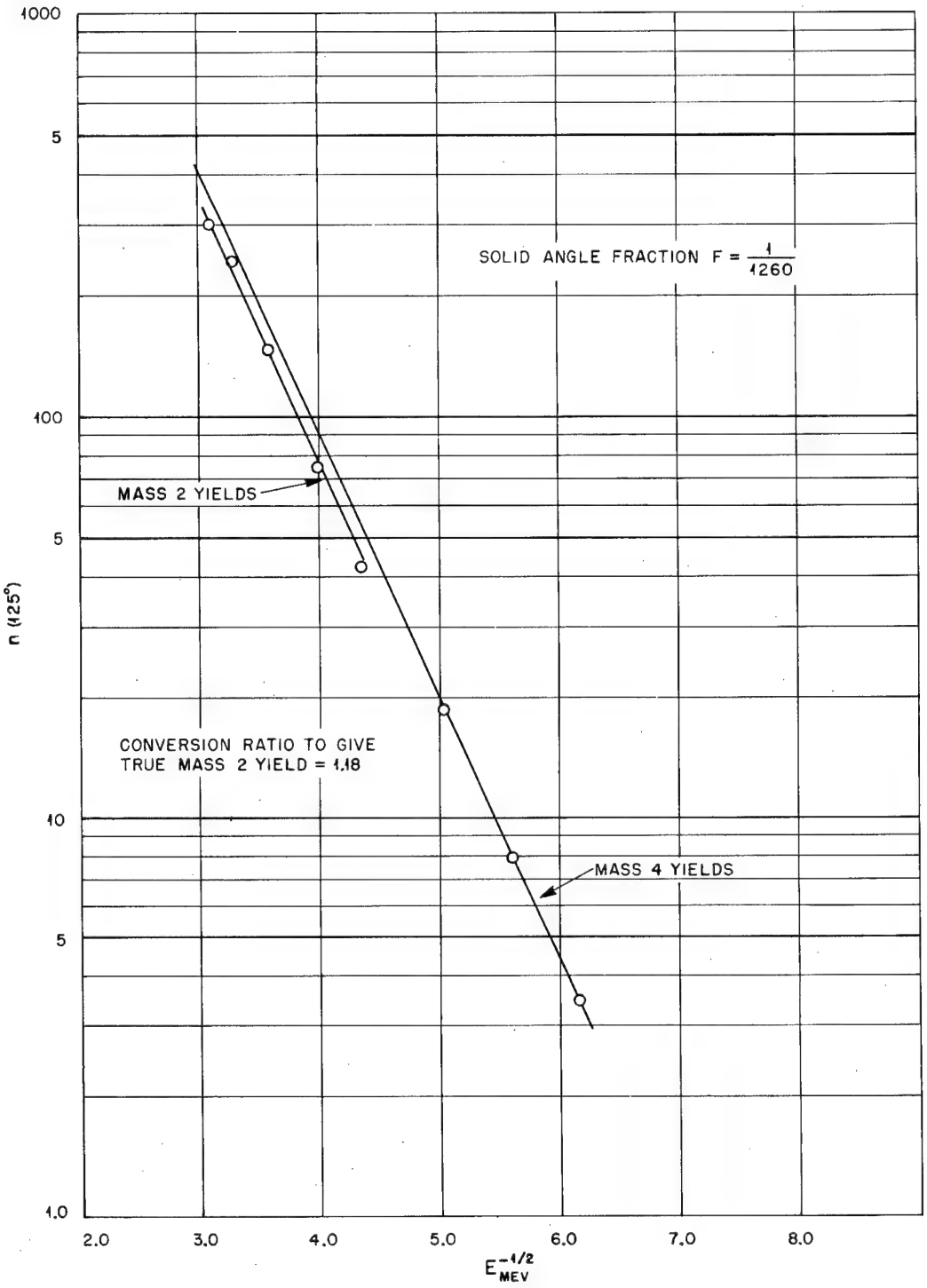

Figure 27. Excitation curve measurements of higher energies (30 kev−150 kev).

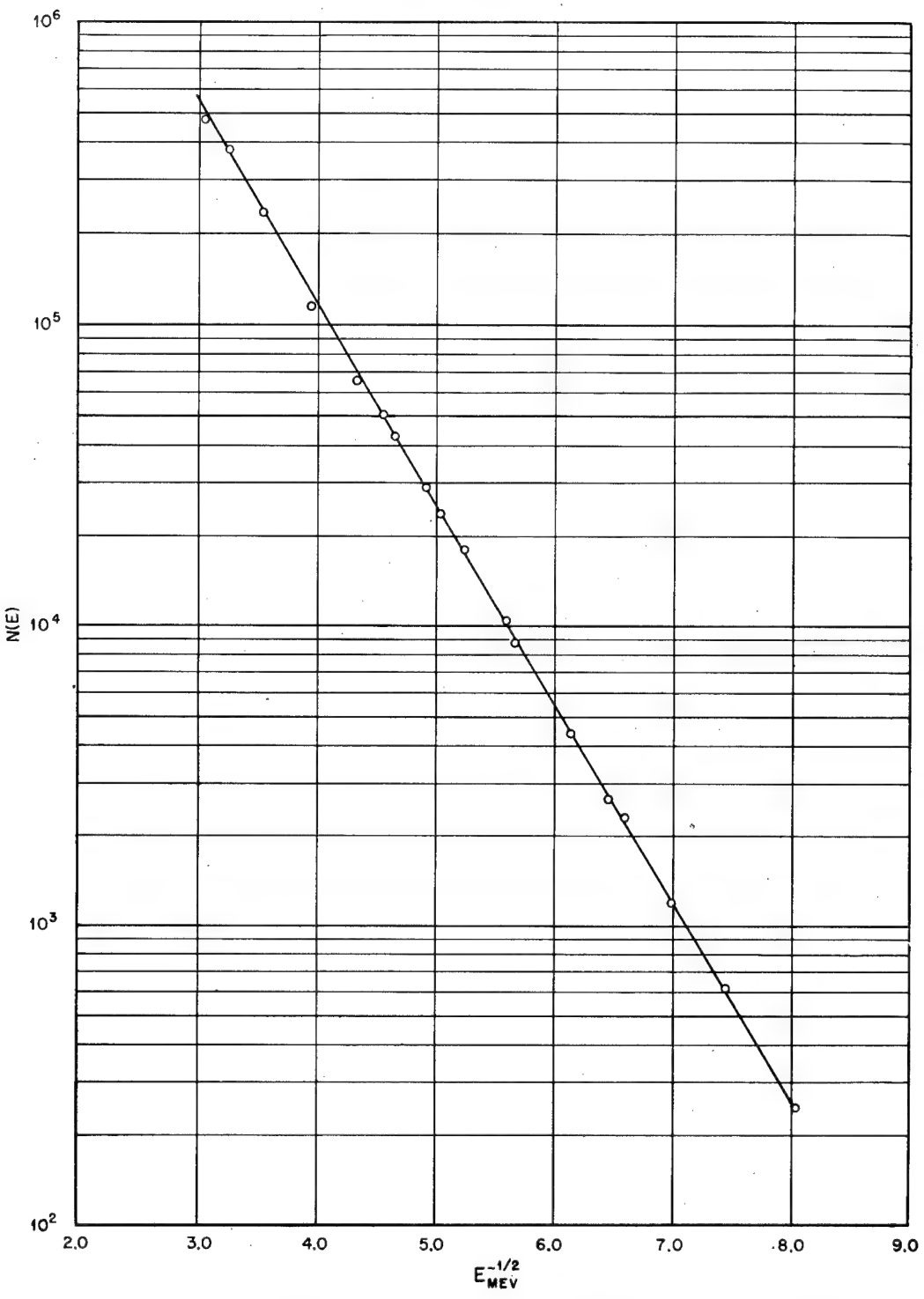

Figure 28. Complete excitation curve D + D, proton emission, 15−105 kev.

Gamow plot: Analytic representation $\log_{10} N(E) = 7.72 - 0.660\ E^{-1/2}_{Mev}$

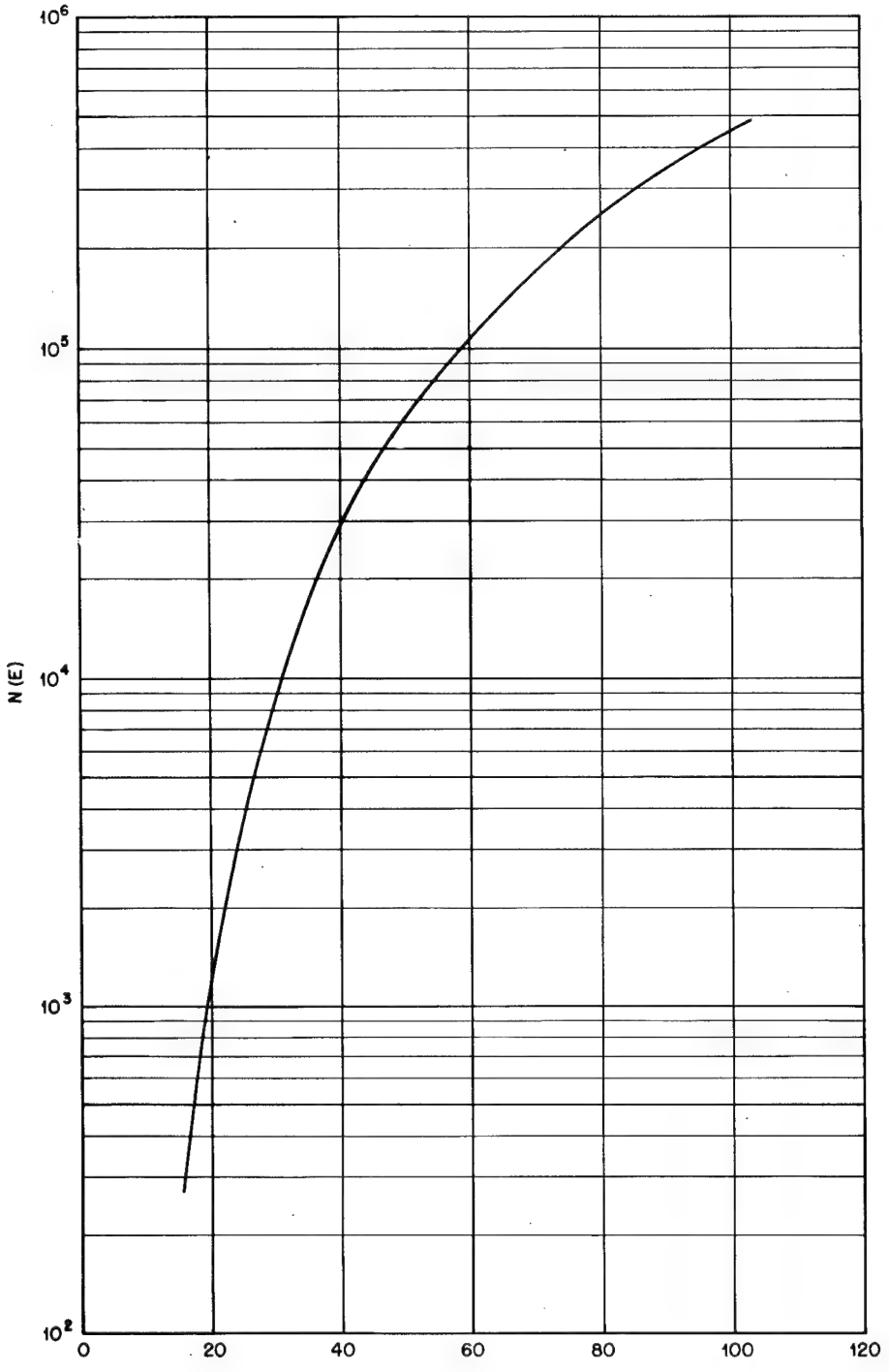

Figure 29. Complete excitation curve, 15 kev−105 kev, N(E) vs. E.

in the beam is, in general, probably not more than 1%. The solid angle fraction F was determined by measuring the counter windows with a comparator, and by carefully determining their distance from the target. The error in F is considered to be about ±2%. The combination of these factors leads to an aggregate error in the thick target yield amounting to ±4% at most energies, but reaching a value as high as ±8% at the lowest energy (15 kev) because of the very low yield.

In deriving cross sections from the values of N(E), one introduces a further small error, perhaps 3% or so, through differentiating the yield curve to find dN/dE. But the associated values of dE/ex are very uncertain, and it is impossible to assign a probable error to the values of the cross sections which will now be derived.

Cross Sections

As was stated at the beginning of this report, the cross section at any energy E is given by:

$2.38.10^{-6}$ (dN/dE)(dE/dx)barns, where dN/dE and dE/dx are measured in specified units (cf. p. 1). To evaluate dN/dE from the experimental values of N(E), two methods have been employed, and are described below.

(a) Direct Method. In Table 1 are given the observed values of N(E) at various energies E. Taking two adjacent energies E_1 and E_2, one finds the value ΔN of the difference $[N_1(E_1) - N_2(E_2)]$ between the yields. Denoting by ΔE the quantity $E_1 - E_2$, the quotient $\Delta N/\Delta E$ represents the value of dN/dE at some mean energy E. The logical choice of E is defined by the 'Gamow' plot (Figure 28) of log N(E) vs. $E^{-\frac{1}{2}}$. Since this is a straight line, it is appropriate to put

$$E^{-\frac{1}{2}} = \tfrac{1}{2}(E_1^{-\frac{1}{2}} + E_2^{-\frac{1}{2}}).$$

The evaluation of $\Delta N/\Delta E$ and of E is set out in Table 2 below. In Table 3 which follows, $\sigma(E)$ and the product $E \cdot \sigma(E)$ are derived. The latter quantity is of interest in comparing experiment with theory (see later).

Table 2.

E_1	$N_1(E)$	E_2	$N_2(E_2)$	ΔN	ΔE	$\Delta N/\Delta E$	$E^{-\frac{1}{2}}$	E
15.4	$2.53.10^2$	18.1	$6.40.10^2$	$3.87.10^2$	2.7	$1.43.10^2$	7.75	16.7
20.5	$1.21.10^3$	23.0	$2.36.10^3$	$1.15.10^3$	2.5	$4.60.10^2$	6.79	21.7
23.8	$2.79.10^3$	26.4	$4.43.10^3$	$1.64.10^3$	2.6	$6.31.10^2$	6.32	25.1
30.6	$8.88.10^3$	31.6	$1.03.10^4$	$1.42.10^3$	1.0	$1.42.10^3$	5.67	31.2
35.6	$1.80.10^4$	39.6	$2.41.10^4$	$6.1.10^3$	4.0	$1.53.10^3$	5.16	37.7
40.9	$2.93.10^4$	45.6	$4.32.10^4$	$1.39.10^4$	4.7	$2.97.10^3$	4.81	43.3
47.7	$5.13.10^4$	52.8	$6.59.10^4$	$1.46.10^4$	5.1	$2.87.10^3$	4.47	50.1
63.2	$1.17.10^5$	79.2	$2.32.10^5$	$1.15.10^5$	16.0	$7.20.10^3$	3.77	70.5
95.0	$3.85.10^5$	105.6	$4.78.10^5$	$9.3.10^4$	10.6	$8.77.10^3$	3.16	100.

E_1, E_2 in kev N_1, N_2 in protons per microcoulomb $E^{-\frac{1}{2}}$ in $(\text{Mev})^{-\frac{1}{2}}$

(b) Analytic Method. Because of the apparently perfect linearity of the plot of log N(E) vs. $E^{-\frac{1}{2}}$ (Figure 28), an analytic representation of the thick target yield was possible, of the form:

$$\log_{10} N(E) = A - B \cdot E_{\text{Mev}}^{-\frac{1}{2}}.$$

Then, by differentiation,

$$\frac{dN}{dE}_{\text{kev}} = 1.152\ B.E_{\text{Mev}}^{-\frac{3}{2}} \cdot N(E) \times 10^{-3}.$$

Table 3.

E	$\frac{\Delta N}{\Delta E}$	$\frac{dE}{dx}$	$\frac{\Delta N}{\Delta t} \cdot \frac{dE}{dx}$	$\sigma(E)$	$E \cdot \sigma(E)$	$E^{-1/2}$
16.7	$1.43.10^2$	0.40	$0.57.10^2$	$1.35.10^{-4}$	$2.25.10^{-3}$	7.75
21.7	$4.60.10^2$	0.48	$2.21.10^2$	$5.26.10^{-4}$	$1.14.10^{-2}$	6.79
25.1	$6.31.10^2$	0.52	$3.29.10^2$	$7.82.10^{-4}$	$1.96.10^{-2}$	6.32
31.2	$1.42.10^3$	0.59	$8.96.10^2$	$2.13.10^{-3}$	$6.65.10^{-2}$	5.67
37.7	$1.53.10^3$	0.66	$1.01.10^3$	$2.40.10^{-3}$	$9.05.10^{-2}$	5.16
43.3	$2.97.10^3$	0.71	$2.11.10^3$	$5.02.10^{-3}$	$2.17.10^{-1}$	4.81
50.1	$2.87.10^3$	0.77	$2.21.10^3$	$5.26.10^{-3}$	$2.64.10^{-1}$	4.47
70.5	$7.20.10^3$	0.90	$6.48.10^3$	$1.54.10^{-2}$	1.09	3.77
100.	$8.77.10^3$	1.02	$8.93.10^3$	$2.13.10^{-2}$	2.13	3.16

Table 4.

E	$E^{-1/2}$	N(E)	$E^{-3/2}$	$\frac{dN}{dE}$	$\frac{dE}{dx}$	$\sigma(E)$	$E\ \sigma(E)$
15	8.15	$2.17.10^2$	544	$0.90.10^2$	0.38	$0.81.10^{-4}$	$1.22.10^{-3}$
17.5	7.54	$5.40.10^2$	432	$1.78.10^2$	0.42	$1.77.10^{-4}$	$3.10.10^{-3}$
20	7.07	$1.13.10^3$	354	$3.04.10^2$	0.46	$3.32.10^{-4}$	$6.64.10^{-3}$
25	6.32	$3.4.10^3$	253	$6.54.10^2$	0.52	$8.1.10^{-4}$	$2.03.10^{-2}$
30	5.77	$8.00.10^3$	192	$1.17.10^3$	0.58	$1.61.10^{-3}$	$4.83.10^{-2}$
35	5.34	$1.54.10^4$	153	$1.80.10^3$	0.63	$2.68.10^{-3}$	$9.40.10^{-2}$
40	5.00	$2.55.10^4$	125	$2.42.10^3$	0.68	$3.91.10^{-3}$	$15.6.10^{-2}$
45	4.72	$3.90.10^4$	105	$3.11.10^3$	0.72	$5.33.10^{-3}$	$2.40.10^{-1}$
50	4.47	$5.80.10^4$	89.4	$3.94.10^3$	0.76	$7.09.10^{-3}$	$3.55.10^{-1}$
60	4.09	$1.04.10^5$	68.1	$5.39.10^3$	0.83	$1.06.10^{-2}$	$6.36.10^{-1}$
70	3.78	$1.65.10^5$	53.9	$6.75.10^3$	0.89	$1.43.10^{-2}$	1.00
80	3.54	$2.35.10^5$	44.3	$7.90.10^3$	0.94	$1.76.10^{-2}$	1.41
90	3.33	$3.25.10^5$	36.9	$9.12.10^3$	0.98	$2.12.10^{-2}$	1.91
105	3.08	$4.80.10^5$	29.3	$1.07.10^4$	1.03	$2.62.10^{-2}$	2.75

Using the method of least squares, the parameter B was found to be 0.660, so that:

$$\left(\frac{dN}{dE}\right)_{kev} = 0.760.E^{-3/2} \cdot N(E) \times 10^{-3} \text{ protons per kev.}$$

Values of dN/dE derived from this formula could then be inserted in the equation for $\sigma(E)$. The working is set out in the following table:
In Table 4, the values of N(E) are taken from the full line drawn through the experimental points in Figure 28. In Tables 3 and 4, the values of dE/dx are taken from LAMS-392; for the sake of completeness the curve showing the variation of dE/dx with energy is reproduced in Figure 30 of this report.

Figure 31 represents the variation of $\sigma(E)$ with E. The full curve corresponds to the values given by the analytic method, and the individual points are those obtained in Table 3 by the direct method. It should be noted that the nine points of Table 3 are obtained from eighteen observed values of N(E), by taking differences in pairs. A small error in either or both values of N(E) leads to a large error in

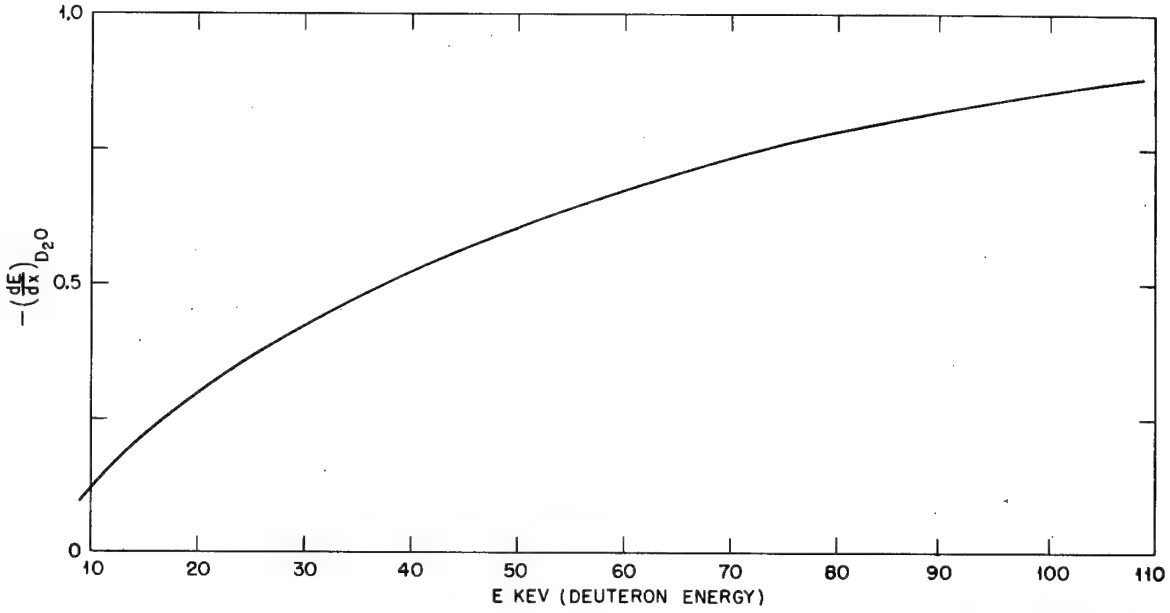

Figure 30. Energy loss of deuterons in D_2O. $\frac{dE}{dx}$ in kev per cm in D_2O vapor at 1 mm pressure, 15°C.

$\sigma(E)$. The deviation of these points from the smooth curve is therefore not unduly great, and it is clear that the best line through them will differ very little from the curve derived analytically.

Comparison with Theory.

On the bias of the Breit-Wigner formula, the cross section is given by:

$$\sigma(E) = \text{const.} \times \frac{1}{E} \times P(E), \qquad \text{where } P(E) \text{ is the probability that}$$

the colliding neuterons will penetrate the potential barrier which separates them. At low energies ($E \ll$ barrier height) this formula takes the simple form:

$$\sigma(E) = \text{const.} \times \frac{1}{E} \times e^{-1.403E^{-1/2}}, \qquad E^{-1/2} \text{ being expressed in } (\text{Mev})^{-1/2}.$$

Thus, if this relation is obeyed, one may write:

$$\log_e \left[E \cdot \sigma(E)\right] = \text{const.} \; -1.403E^{-1/2}$$

or

$$\log_{10} \left[E \cdot \sigma(E)\right] = \text{const.} \; -0.608E^{-1/2}$$

In Figure 32 a plot of $\log [E \cdot \sigma(E)]$ vs. $E^{-1/2}$ is made. Its slope is 0.662 instead of the 0.608 required by the theory. (A line of the theoretical slope is indicated on the figure.)

Although the difference between theory and experiment is considerable, it is by no means outside the uncertainties of theory or of experiment. The one large source of doubt in the experiments lies in the use of dE/dx to find $\sigma(E)$. On the other hand, from the theoretical point of view it is hard to say what should be the correct power of E preceding the exponential in the cross section formula. If one puts $1/E^{1/2}$ in the place of 1/E, then the theoretical slope becomes greater than the experimental, whereas before it was less, as may be seen from Figure 32.

For a fuller discussion of the problem, reference should be made to the article by E. J. Konopinski in the Technical Series (Vol. 3, ch. 7).

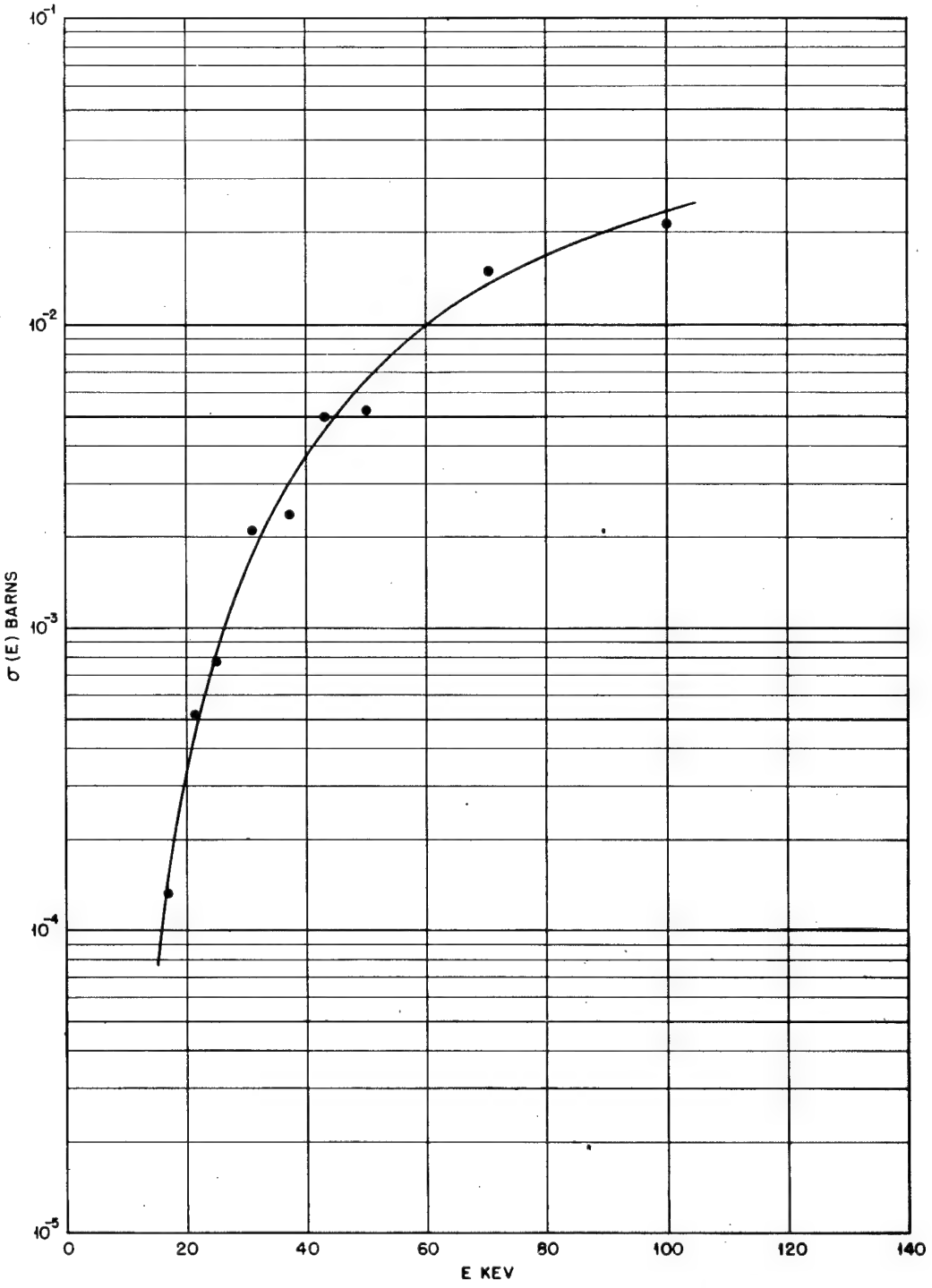

Figure 31. D + D cross section, 15 kev to 105 kev (proton emission).

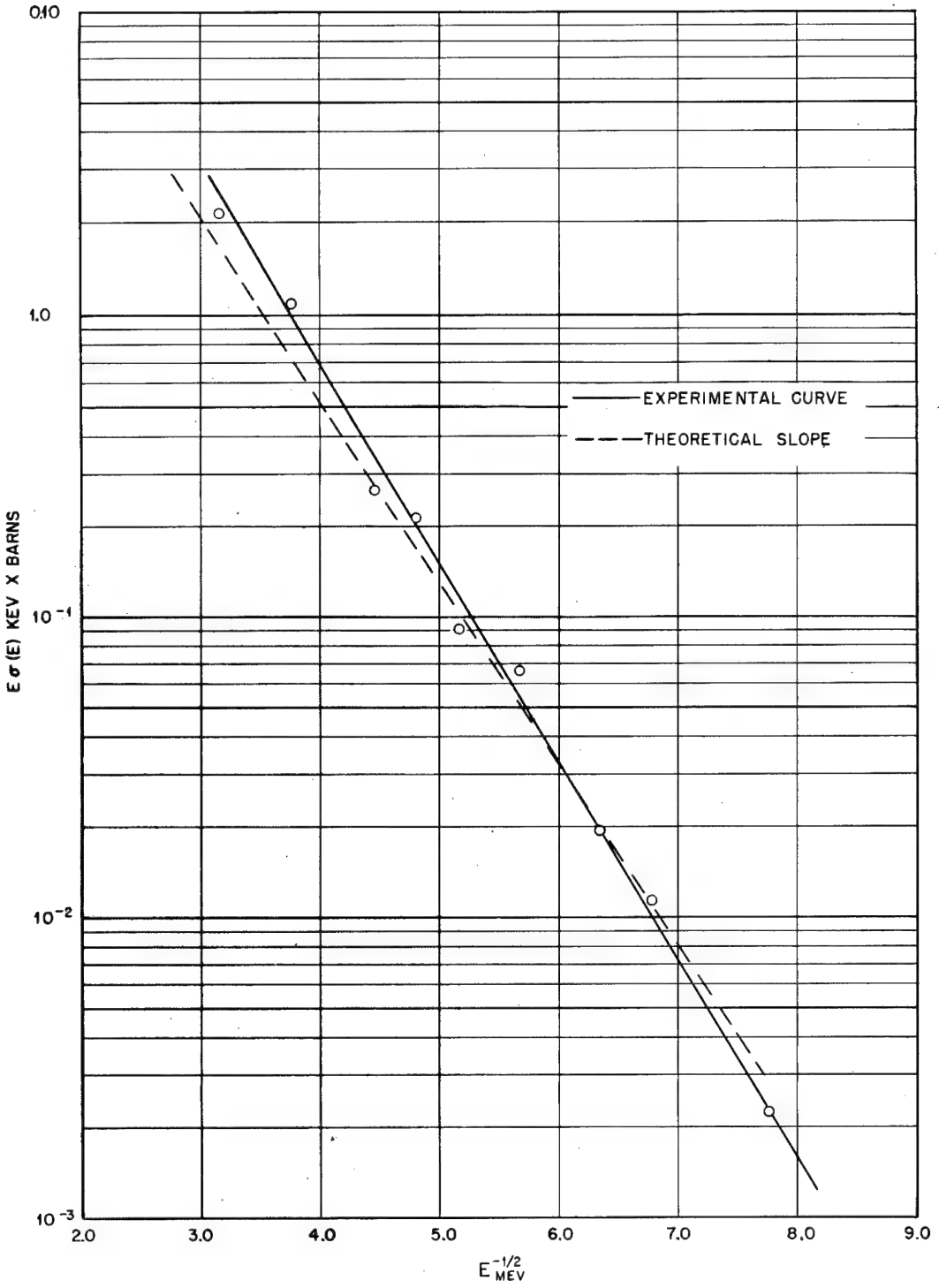

Figure 32. Gamow plot: log $[E\,\sigma(E)]$ vs. $E^{-1/2}$ theoretically, $\sigma(E) = \text{const.}\,\frac{1}{E}\cdot e^{-1.403\,E^{-1/2}}$

Concluding Remarks

No experiments have been made on the alternative nuclear reaction

$$D + D \rightarrow He_3 + n + 3.25 \text{ Mev.}$$

It would have been very desirable to study this process, since in reality a comparison with theory demands a knowledge of the total cross section for the D - D interaction, and the theoretical considerations of the preceding section are based on the assumption of a constant branching ratio. The difficulties in the way of detecting, with good accuracy, either the He_3 or the neutrons are, however, rather great. The He_3 have a range of only 4.3 mm for these bombarding energies near to zero, so that to detect them one must have a counter the air equivalent of whose window is considerably less than this. On the other hand, the detection of the neutrons must depend upon an inefficient secondary process, and the low primary reaction yield at these energies makes for very low counting rates. The problems are by no means insuperable, and a full study of the D + D reaction must certainly deal with this alternative reaction.

In addition, if thick-target yield measurements are to be translated with any certainty into values for cross sections, a far better knowledge of dE/dx for deuterons in heavy ice is required. It is considered that the experiments described in this report give a fairly reliable measure of the thick-target yield for the D(D,p)T reaction from 15 to 105 kev, but the values here advanced for cross sections should be regarded with suspicion.

APPENDIX

Here are collected various equations and calculations relevant to the experiments and their interpretation.

A. Transformation of Angles From Laboratory to Center-of-Gravity

If θ is the angle measured in the laboratory, and θ' is the corresponding angle in the center-of-gravity system, then:

$$\sin(\theta' - \theta) = a \cdot \sin\theta,$$

where

$$a^2 = \frac{m_1 m_3}{m_2 m_4} \cdot \frac{1}{1 + \frac{Q}{E}\frac{m_1 + m_2}{m_2}}$$

m_1 = mass of incident particle.
m_2 = mass of bombarded particle.
m_3 = mass of observed particle.
m_4 = mass of remaining particle.
Q = energy release of reaction.
E = energy of incident particle.

An approximate expression for $\sin(\theta' - \theta)$ is:

$$\sin(\theta' - \theta) = \sin\theta \times \left(\frac{m_1 m_3}{m_4 M}\right)^{1/2} \left(\frac{E}{Q}\right)^{1/2} \left[1 - \frac{1}{2}\left(\frac{m_2}{M}\right)\left(\frac{E}{Q}\right) + \frac{3}{8} \cdot \left(\frac{m_2}{M}\right)^2 \cdot \frac{E^2}{Q} - \cdots\right]$$

where

$$M = m_1 + m_2 = m_3 + m_4$$

B. The Correction Factor $g(\theta)$.

$$g(\theta) = \frac{d(\cos\theta)}{d(\cos\theta')} = \frac{(1 - a^2\sin^2\theta)^{1/2}}{\left[a \cdot \cos\theta + (1 - a^2\sin^2\theta)^{1/2}\right]^2}$$

Approximate expression:

$$g(\theta) = 1 - 2a\cos\theta + a^2\left(3 - \frac{5}{2}\sin^2\theta\right) + \cdots$$

$$g(\theta) = 1 - 2\cos\theta\left(\frac{m_1 m_3}{m_2 m_4}\right)^{1/2}\left(\frac{m_2}{m_1 \quad m_2}\right)^{1/2}\left(\frac{E}{Q}\right)^{1/2}$$

$$+ \left(3 - \frac{5}{2}\sin^2\theta\right)\left(\frac{m_1 m_3}{m_2 m_4}\right)\left(\frac{m_2}{m_1 \quad m_2}\right)\left(\frac{E}{Q}\right) + \text{---}$$

C. Errors due to observation at $\cos^{-1}\left(\pm\frac{1}{\sqrt{3}}\right)$ in the laboratory

From equations (3) and (4) in the text (p. 10) it follows that one may write:

$$n(\theta) = \frac{1}{g(\theta)}\; n'(90°)\left[1 + A(E)\cos^2\theta'\right]$$

We wish to study the dependence of $n(\theta)$ on small changes of θ in the neighborhood of $\theta = 54°44'$ and $125°16'$. Since $n'(90°)$ is not a function of θ, we may write:

$$\frac{n(\theta)}{n'(90°)} = R(\theta) = \left[g(\theta)\right]^{-1}\;\left[1 + A(E)\cos^2\theta'\right]$$

Now from paragraph B above, we have:

$$g(\theta) \sim 1 - 2a\quad\cos\theta + a^2\left(3 - \frac{5}{2}\sin^2\theta\right)$$

whence

$$g(\theta)^{-1} \sim 1 + 2a\cos\theta + a^2\left(1 - \frac{3}{2}\sin^2\theta\right)$$

In the neighborhood of $54°44'$ and $125°16'$, $\sin^2\theta \sim \frac{2}{3}$, so that $\left(1 - \frac{3}{2}\sin^2\theta\right)$ is very nearly zero. Moreover, we may neglect this term in differentiation since it is always multiplied by the small factor a^2. Thus it is permissible to write:

$$R \sim \left[1 + A(E)\cos^2\theta'\right]\;(1 + 2a\,.\,\cos\theta) \text{ simply.}$$

Differentiating,

$$\Delta R \sim -2A(E)\cos\theta'\,\sin\theta'\,\Delta\theta'\,(1 + 2a\,.\,\cos\theta) - 2a\,.\,\sin\theta\,\Delta\theta\,(1 + A(E)\cos^2\theta')$$

Now

$$\sin\theta'\,\Delta\,\theta' = \frac{\sin\theta\Delta\,\theta}{g(\theta)} \sim (1 + 2a\cos\theta)\sin\theta\,\Delta\theta$$

Thus

$$\Delta R \sim -2A(E)\cos\theta'\,\sin\theta\Delta\theta\,(1 + 2a\cos\theta)^2 - 2a\sin\theta\Delta\theta\left[1 + A(E)\cos^2\theta'\right]$$

$\Delta\theta$ is the small angle $(\theta' - \theta)$ representing the shift from the center-of-gravity to the laboratory system. Thus we may write:

$$\cos\theta' \sim \cos\theta - \sin\theta\,\Delta\theta$$

$$\cos^2\theta' \sim \cos^2\theta - 2\sin\theta\cos\theta\,\Delta\theta.$$

Thus,

$$\Delta R \sim -2\sin\theta\,\Delta\theta\Big\{A(E)\,.\,(1 + 2a\cos\theta)^2\,(\cos\theta - \sin\theta\Delta\theta) + a\left[1 + A(E)\cos^2\theta - 2A(E)\sin\theta\cos\theta\,\Delta\theta\right]\Big\}$$

$$\sim -2\sin\theta\Delta\,\theta\Big\{A(E)\cos\theta\,(1 + 2a\cos\theta)^2 + a\left[1 + A(E)\cos^2\theta\right]\Big\}$$

$$+ 2\sin^2\theta\,\Delta\theta^2\Big\{(1 + 2a\cos\theta)^2\,A(E) + 2a\,A(E)\cos\theta\Big\}$$

Neglecting powers of a above the first, this becomes:

$$\Delta R \sim -2 \sin\theta\, \Delta\theta \left[A(E) \cos\theta + 5a\, A(E) \cos^2\theta + a\right] + 2A(E) \sin^2\theta\, \Delta\, \theta^2 \left[1 + 6a \cos\theta\right]$$

Inserting $\sin\theta = \frac{\sqrt{2}}{\sqrt{3}}$; $\cos\theta = \frac{1}{\sqrt{3}}$,

$$\Delta R \sim -\frac{2\sqrt{2}}{\sqrt{3}} \Delta\theta \left[\pm \frac{A(E)}{\sqrt{3}} + \frac{5a\, A(E)}{3} + a\right] + \frac{4}{3} A(E) \Delta\, \theta^2 \left[1 + 2\sqrt{3}\, a\right]$$

At the highest energy used (105 kev),

$$a \sim \frac{1}{15} \qquad A(E) \sim 0.45$$

Thus

$$\Delta R \sim -1.64\, \Delta\theta \left[\pm 0.260 + 0.049 + 0.066\right] + 0.60\, \Delta\theta^2 \left[1 \pm 0.23\right]$$

Now $\Delta\theta$ is the value of $(\theta' - \theta)$ at 105 kev, $\sin^{-1} \frac{1}{\sqrt{3}}$, and this is $\sim 3°$ or $\frac{1}{19}$ radian.

Inserting this value, we find:

$$\Delta R\ (55°) = -0.031, \text{ and } R\ (55°) = 1.25$$

$$\Delta R\ (125°) = 0.015, \text{ and } R\ (125°) = 1.06$$

The percentage errors introduced by observing at angles $\cos^{-1}\left(\pm\frac{1}{\sqrt{3}}\right)$ in the laboratory are thus -2.5% and + 1.4 % respectively.

D. Derivation of a(E) from A(E)

(i) Direct Method.

The thick-target yield is represented in the center-of-gravity system by:

$$N(E) = C(E) + D(E) \cos^2\theta'$$

$$= C(E) \left[1 + \frac{D(E)}{C(E)} \cos^2\theta'\right]$$

$$= C(E) \left[1 + A(E) \cos^2\theta'\right]$$

Differentiating:

$$\frac{dN}{dE} = \frac{dC}{dE} + \frac{dD}{dE} \cos^2\theta'$$

$$= \frac{dC}{dE} \left[1 + \frac{dD/dE}{dC/dE} \cos^2\theta'\right]$$

$$= \text{const} \left[1 + a\,(E) \cos^2\theta'\right]$$

Thus

$$a(E) = \frac{dD/dE}{dC/dE}$$

(ii) Konopinski's Method

It was pointed out by Konopinski that the above method was undesirable, in that a(E) was evaluated as the ratio of two differentials. He has presented a method (cf. Technical Series, Vol. 3, ch. 7) in

which advantage has been taken of the closeness of a(E) to A(E). The method is outlined here, using the symbolism employed in the rest of this report. From equation (7) in the test, we have:

$$n_{\theta'}(E) = F \cdot N(E) \cdot \frac{1 + A(E)\cos^2\theta'}{1 + \frac{1}{3}A(E)}$$

Differentiating,

$$\frac{1}{F}\frac{d}{dE}\left[n_{\theta'}(E)\right] = \frac{dN}{dE}\frac{1 + A(E)\cos^2\theta'}{1 + \frac{1}{3}A(E)} + N(E)\frac{dA}{dE}\cdot\frac{\cos^2\theta' - 1/3}{\left[1 + \frac{1}{3}A(E)\right]^2}$$

But by the definition of a(E), we have:

$$\frac{1}{F}\frac{d}{dE}\left[n_{\theta'}(E)\right] \equiv \frac{dN}{dE}\cdot\frac{1 + a(E)\cos^2\theta'}{1 + \frac{1}{3}a(E)}$$

The identity of the above two expressions holds for all values of θ'; by equating separately the constant terms and the coefficients of $\cos^2\theta'$, we arrive at the following relations:

$$\frac{dN}{dE}\cdot\frac{1}{1 + \frac{1}{3}A(E)} - N\frac{dA}{dE}\cdot\frac{1}{3\left[1 + \frac{1}{3}A(E)\right]^2} = \frac{dN}{dE}\cdot\frac{1}{1 + \frac{1}{3}a(E)}$$

$$\frac{dN}{dE}\cdot\frac{A}{1 + \frac{1}{3}A(E)} + N\frac{dA}{dE}\cdot\frac{1}{\left[1 + \frac{1}{3}A(E)\right]^2} = \frac{dN}{dE}\cdot\frac{a(E)}{1 + \frac{1}{3}a(E)}$$

Dividing the second equation by the first:

$$a(E) = \frac{\frac{dN}{dE}\cdot\frac{A(E)}{1 + \frac{1}{3}A(E)} + N\frac{dA}{dE}\cdot\frac{1}{\left[1 + \frac{1}{3}A(E)\right]^2}}{\frac{dN}{dE}\cdot\frac{1}{1 + \frac{1}{3}A(E)} - N\frac{dA}{dE}\cdot\frac{1}{3\left[1 + \frac{1}{3}A(E)\right]^2}}$$

$$= A(E)\frac{1 + \frac{N\,dA/dE}{A\,dN/dE}\cdot\frac{1}{1 + \frac{1}{3}A(E)}}{1 - \frac{N\,dA/dE}{3\,dN/dE}\cdot\frac{1}{1 + \frac{1}{3}A(E)}}$$

or approximately:

$$a(E) \sim A(E) + \frac{N(E)}{dN/dE}\cdot\frac{dA}{dE}$$

END OF DOCUMENT